Joana Micaelo Grilo

Bachelor of Science in Biomedical Engineering

NM-MRI for treatment evaluation of Parkinson's Disease patients

Dissertation submitted in partial fulfillment
of the requirements for the degree of

Master of Science in
Biomedical Engineering

Adviser: Rita G. Nunes, Assistant Professor,
Instituto Superior Técnico, University of Lisbon

Co-adviser: Sofia Reimão, Neuroradiologist,
Faculty of Medicine, University of Lisbon
and Hospital de Santa Maria,
Centro Hospitalar Lisboa Norte

Examination Committee

Chairperson: Doctor Carla Maria Quintão Pereira
Raporteur: Doctor Sónia Isabel Domingos Marreiros Gonçalves
Member: Doctor Rita Homem de Gouveia Costanzo Nunes

FACULDADE DE
CIÊNCIAS E TECNOLOGIA
UNIVERSIDADE NOVA DE LISBOA

September, 2017

NM-MRI for treatment evaluation of Parkinson's Disease patients

This document was created using the (pdf)LaTeX processor, based in the "novathesis" template[1], developed at the Dep. Informática of FCT-NOVA [2].
[1] https://github.com/joaomlourenco/novathesis [2] http://www.di.fct.unl.pt

I believe firmly that a good education is the most cherished gift an individual can receive.

William Rand Kenan, Jr.

Acknowledgements

Foremost, I would like to express my sincere gratitude to my advisers Prof. Rita Nunes and Dr. Sofia Reimão for all the guidance, sympathy, knowledge and continuous support. I could not have imagined having better advisers. You gave me motivation when I needed it the most. Thank you for everything.

I would like to thank the Faculty of Sciences and Technology of NOVA University of Lisbon for providing me an immense knowledge.

I would also like to thank the Institute for Systems and Robotics of Instituto Superior Técnico and all the amazing people that I got to meet there for the wonderful welcome and inclusion. A special thanks to my lab partner and great friend Ana Fouto for all the help, the snack breaks much needed to regain energy and the reprehensible but at the same time kind words when I lost focus.

I would also like to thank my parents for providing me everything I needed and more, a great education, unconditional love, freedom and trust that I would do my best throughout these five years. Thank you to my beautiful sisters for the friendship and motivation. Also, a special thank to my boyfriend for always believing in me when I often doubted my abilities and for all the support and help.

Last but not least, I would like to thank the best girls in the world: Kateryna, Marta and Teresa, without whom these five years would not have been so amazing. Thank you for everything that we shared, all the nights studying and partying, and for shaping me into who I am today as a person.

Abstract

T1-weighted fast spin echo magnetic resonance imaging (MRI) sequences are able to depict neuromelanin (NM)-containing structures, such as the *Substantia nigra* (SN), as hyper-intense signal areas. NM-MRI can accurately discriminate Parkinson's Disease (PD) patients from controls and could potentially be used to evaluate the effects of PD treatment - either surgery or medication. PD patients that are treated with Deep Brain Stimulation (DBS) can only undergo 1.5T MRI sequences with specific conditions that prevent the tissues surrounding the neurostimulators from overheating. However, NM-MRI sequences are usually not applied at 1.5T due to worse image quality. Nevertheless, it would be interesting to study how DBS and medication influence the NM signal as a path for a better understanding of the disease and to potentially evaluate the progression of PD after the surgical intervention.

Firstly in this work, a NM-MRI sequence was adapted for scanning patients with implanted DBS systems at 1.5T. To evaluate the performance of the sequence, images were taken on the same day with 1.5T and 3T MRI systems. The contrast ratio of both sequences was evaluated and SN areas were measured resorting to a semi-automatic segmentation algorithm. The assessment of these measurements revealed a good agreement between the developed sequence and the original 3T sequence.

A second study was carried out, in which SN areas of PD *de novo* patients were evaluated before and after two months of initiating pharmacological treatment. The median SN area tended to be increased after treatment, suggesting a potential increase of NM related to dopamine therapy.

In conclusion, this work presented the first 1.5T NM-MRI sequence that enables SN area measurement of patients with implanted neurostimulators, for further investigation of this method as a diagnostic tool for assessment of disease progression and to better understand clinical effects on NM-MRI and PD itself.

Keywords: NM-MRI, 1.5T sequence, Deep Brain Stimulation, Parkinson's Disease, Substantia Nigra

Resumo

A técnica de imagem por ressonância magnética (IRM) recorrendo a sequências *fast spin echo* permite distinguir estruturas relacionadas com Doença de Parkinson (DP), como a *Substantia nigra* (SN), devido ao sinal hiper-intenso proveniente da neuromelanina (NM). Estas imagens discriminam pacientes com DP de controlos e podem potencialmente avaliar os efeitos da terapêutica - tanto medicação como cirurgia. Pacientes com DP que são tratados com estimulação profunda, para evitar o sobreaquecimento dos tecidos em contacto com os elétrodos durante exames subsequentes à cirurgia, apenas podem ser monitorizados a 1.5T. Apesar das imagens a 1.5T apresentarem pior qualidade, seria interessante estudar a influência da estimulação no sinal da NM, na medida em que poderia contribuir para a monitorização dos doentes após a cirurgia.

Neste trabalho, foi adaptada uma sequência sensível a NM para permitir a monitorização a 1.5T de doentes com neuroestimuladores implantados. Para avaliar o seu desempenho, foram efetuados exames a 3T e 1.5T no mesmo dia. O contraste das mesmas foi avaliado e utilizou-se uma ferramenta de segmentação semiautomática para medir as áreas da SN. As áreas medidas com a sequência desenvolvida e a sequência original a 3T mostraram uma boa concordância.

Adicionalmente, as áreas da SN de pacientes DP *de novo* foram medidas antes e após dois meses de iniciar a medicação. Verificou-se uma tendência de aumento da SN após tratamento, sugerindo um potencial aumento da neuromelanina relacionado com a terapia de dopamina.

Para concluir, este trabalho apresentou a primeira sequência de IRM sensível a neuromelanina que permite medir as áreas da SN de pacientes de DP com neuroestimuladores implantados. Esta sequência pode vir a ser utilizada como uma ferramenta de avaliação da progressão da doença e contribuir para um melhor entendimento dos efeitos da terapêutica neste tipo de imagens assim como aprofundar os conhecimentos da DP.

Palavras-chave: IRM, Neuromelanina, Neuroestimuladores, Doença de Parkinson, Substantia Nigra

Contents

List of Figures

List of Tables

Acronyms

CI	Confidence Intervals.
CR	Contrast Ratio.
DA	Dopamine.
DBS	Deep Brain Stimulation.
DSC	Dice Similarity Coefficient.
FA	Flip Angle.
FID	Free Induction Decay.
FOV	Field of View.
FSE	Fast Spin Echo.
FWHM	Full Width at Half Maximum.
GE	Gradient Echo.
ICC	Intraclass Correlation Coefficient.
IPG	Implantable Pulse Generator.
MAO	MonoAmine Oxidation.
MR	Magnetic Resonance.
MRI	Magnetic Resonance Imaging.
MT	Magnetization Transfer.
NM	Neuromelanin.
PD	Parkinson's Disease.
PDn	Proton Density.
PI	Parallel Imaging.
PPT	Pedunculopontine Tegmental Nucleus.

RF	Radiofrequency.
ROI	Region-of-Interest.
SAR	Specific Absorption Rate.
SE	Spin Echo.
SENSE	SENSitivity Encoding.
SN	*Substantia Nigra*.
SNc	*Substantia Nigra pars compacta*.
SNR	Signal-to-Noise Ratio.
SORS	Slice Selective Off Resonance Sinc.
STC	Saturation Transfer Contrast.
STN	Subthalamic Nucleus.
TE	Time of Echo.
TR	Time of Repetition.
UPDRS	Unified Parkinson's Disease Rating Scale.
WI	Weighted Image.

CHAPTER 1

Introduction

1.1 Motivation

Parkinson's Disease (PD) is a neurodegenerative disorder that affects over 10 million people in the world. This disease is characterized by a progressive loss in motor functions, which translates in incapacitating symptoms such as resting tremor, rigidity, postural instability and others. Even though a cure for PD has not yet been found, it is possible to reduce its symptoms by taking anti-Parkinson medication and/or going through surgery.

A recurrent technique used to improve some of Parkinson's disease symptoms is the electrical stimulation of the Subthalamic Nucleus (STN). However, after implantation of the neurostimulators, said patients become restricted to 1.5T Magnetic Resonance (MR) images of the patient due to the potential over heating in the implanted electrodes on 3T MR scanners, which can cause serious damages to the tissue in contact.

Neuromelanin (NM)-sensitive Magnetic Resonance Imaging (MRI) is a promising technique to allow *in vivo* visualization of the pathological changes in NM-containing structures that occur in degenerative diseases such as PD. PD is accompanied by progressive neuronal loss of the *Substantia Nigra* (SN) neurons. These neurons contain a dark pigment - neuromelanin - whose paramagnetic properties lead to a T1 hyper-intense signal of the SN on NM-MRI. Therefore, this type of imaging has been increasingly used to evaluate PD since it can depict the NM-related contrast.

The majority of studies have applied NM-MRI at 3T due to its improved resolution and signal-to-noise ratio (SNR). However, as it was already mentioned, due to safety reasons PD patients with implanted neurostimulators can only be imaged with 1.5T MRI systems.

1.2 Aim of this work

The overall aim of this work was to assess potential effects of PD therapeutic using NM-MRI.

Having in mind the reduced availability of 3T MRI systems, this work's first goal was to adapt the 3T clinical standard sequence into a 1.5T NM-MRI sequence, which could accurately depict the neuromelanin-corresponding SN area. In an initial stage, the general 1.5T NM-MRI sequence's feasibility was assessed through comparison with the currently used 3T sequence.

A further aim of this work, in order to assess potential efects of DBS on NM-MRI, was to adapt the sequence to safely scan PD patients with implanted neurostimulators. The 1.5T NM-MRI sequence adapted for patients with implanted DBS systems was then compared with the previously developed general 1.5T sequence.

An additional goal was to establish the repeatability of the SN areas obtained with the applied semi-automatic segmentation algorithm, for all tested MRI sequences.

Furthermore, another aim of this work was to enable to uncover the direct effects of medication on the measured NM-SN area of PD patients and, in turn, to obtain a deeper knowledge on the role of dopamine in NM production, potentially building towards a full understanding of PD.

1.3 Thesis Outline

This thesis consists of six different chapters and is followed by an appendix.

In the current chapter, in addition to this outline, it is included the motivation for this work, presenting the problems regarding 3T MRI in PD patients with implanted DBS systems, explaining what is the role of NM-MRI sequences and what is the aim of this study.

The second chapter, *Theoretical Principles and State of the Art*, is a literature review of the most important concepts used in this dissertation, starting with the basic notions of MRI required for understanding the development of a sequence. Also in this chapter is provided an overview of PD, DBS and how they relate. Apart from this, a review on NM-MRI as a diagnostic and research tool for PD is made. Finally, the statistical tests later used in this work are briefly described.

The third chapter marks the beginning of the presentation of the experimental work, discussing the necessary changes applied to the acquisition parameters used to develop the 1.5T NM-MRI sequence. Following this, a characterization of the image processing is made as well as a presentation of the methods used to validate the segmented SN areas against the current gold standard method (manual segmentation).

In the fourth chapter, another study for sequence validation is presented. This time, the validated 1.5T NM-MRI sequence is adapted to be safely used in the examination of patients with implanted DBS systems.

The fifth chapter is dedicated to the influence of another type of PD therapeutic - medication - in the NM present in the SN. It starts with a review on the dopamine metabolism, which is helpful for a better understanding of the results. The NM-MR images of PD patients before and after the initiation of medication are presented and analyzed.

Lastly, in the sixth and final chapter of this dissertation, the conclusions regarding the results obtained are summed up and some suggestions for future studies are presented.

CHAPTER 2

Theoretical Principles and State of the Art

2.1 Magnetic Resonance Imaging

2.1.1 Physical Fundamentals

Magnetic Resonance Imaging is a technique that relies on the Hydrogen nuclei´s magnetic properties. The ^1H nucleus is frequently used in imaging acquisition since it is the most abundant proton in the human body and possesses nuclear spin. Due to this nucleus property, and according to the quantum principles, when the proton is submitted to a magnetic field the spin becomes restricted to one of two discrete directions: parallel (low-energy state) and anti-parallel (high-energy state) to the external magnetic field. Since most of the MR principles can be explained using a classical approach, from now on the model used to describe the MR phenomena will be the classical one.

A nucleus with spin has an axis of rotation that can be represented as a vector with a certain magnitude and orientation. The magnetic moment is parallel to this axis [1]. In the absence of a magnetic field the spins are randomly oriented, which results in a null net magnetization (Figure 2.1).

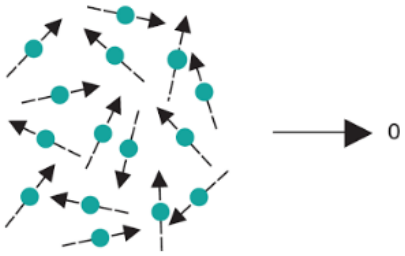

Figure 2.1: Representation of the protons in the absence of an external magnetic field. Their spin vectors are randomly oriented (left side). The sum of these vectors is null (right side). Adapted from [1]

When an external magnetic field is applied to the protons, B_0, the nuclear spins align with B_0 and start to precess around the axis of rotation at a certain rate of resonance. This resonance frequency, also called Larmor frequency, is proportional to the external magnetic field: $\omega_0 = \gamma B_0$, wherein γ is the gyromagnetic constant, specific to each nucleus.

Proton magnetization can be divided into two components - longitudinal and transverse - taking into account their movement. The parallel coordinate (z) to B_0, or longitudinal, is constant with time and positive. The transverse coordinates (x and y), or perpendicular to B_0, are non-null and vary with the precession. In the direction perpendicular to B_0, the spins orientations are randomly distributed whereby the resulting transverse magnetization is null.

When a Radiofrequency (RF) pulse is applied with the Larmor frequency, resonance occurs and there is energy absorption by the nucleus. This energy transfer consists of a shift from the lower state of energy to the higher one. The Flip Angle (FA) defines the angle of rotation of the magnetization from the longitudinal axis to the transverse plane and is proportional to the RF pulse duration and B1 field amplitude. When the RF pulse stops and the system returns to its natural state, relaxation, which is accompanied by an emission of electromagnetic energy, occurs. The signal which originates from this phenomenon is called Free Induction Decay (FID) and it is characterized by the time constant T_2^*. This constant is affected by spin-spin interactions and heterogeneities in B_0 which lead to an acceleration on the dephasing of spins, following the expression:

$$\frac{1}{T_2^*} = \frac{1}{T_2} + \frac{1}{T_{2i}} \tag{2.1}$$

Where the time constant T_2 is tissue specific and describes the relaxation curve of the transverse magnetization, related to spin-spin interaction. T_{2i} is related to the inhomogeneities of the magnetic field. The longitudinal relaxation is the result of the energy transfer from the spins to the net. Its decay curve is characterized by the time constant T_1, which is also tissue specific. This last constant is always greater than T_2 for a given tissue.

2.1.2 MR Pulse Sequences

RF pulse sequences enable the acquisition of MR signals, which contain information about the scanned object. These signals are later digitalized to fill in a matrix, called K–space. In MRI spatial encoding is achieved through the application of gradient fields - frequency and phase encoding. Each line of the K–space corresponds to the data obtained from a single phase encoding gradient and the columns correspond to the frequency encoding gradients. Finally, the inverse Fourier Transform is applied to the K–space to form an image.

MR pulse sequences have many variations, however there are two main base sequences: Spin Echo (SE) and Gradient Echo (GE).

SE sequences consist in the application of a 90° RF pulse followed by a 180° RF pulse (Figure 2.2), or in the case of a Multi-Echo SE sequence, multiple 180° pulses. The initial 90° pulse causes the previously explained resonance. The 180° pulses, echo creators, lead to phase coherence between spins which reverses field heterogeneity effects, enabling a T_2-weighted image acquisition. In conventional SE, the phase encoding gradient is turned on only one time per Time of Repetition (TR) interval, which corresponds to a single line of the K–space being filled per TR interval. Typically MRI sequences are characterized by two parameters: Time of Echo (TE) and TR. TE is the time between the 90° pulse application and the center of the first echo. TR is the time between two excitation pulses, 90°.

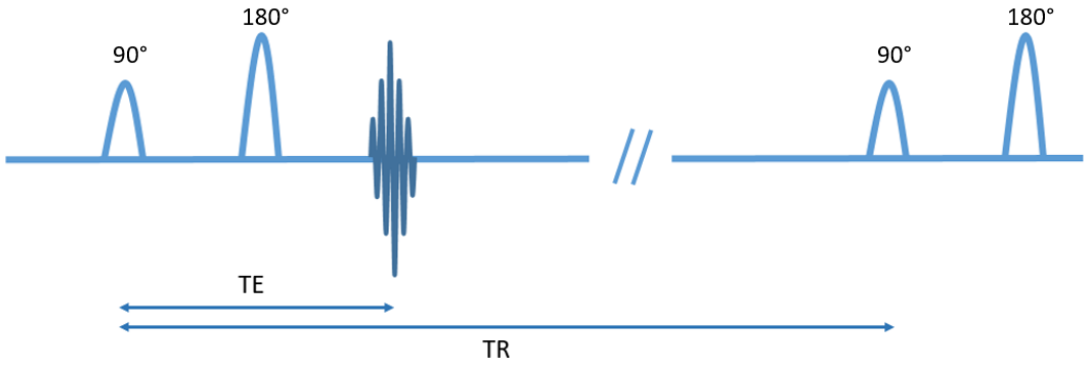

Figure 2.2: Representation of a Spin Echo Sequence. Adapted from [2].

In Fast Spin Echo (FSE) sequences, multiple 180° pulses and echoes follow each 90° pulse. However, unlike Multi-Echo SE, in FSE sequences after each echo, the phase encoding gradient is rewound and a different phase encoding is applied to the following echo (Figure 2.3a). This enables a faster filling of the k-space with reduced number of repetitions (number of TRs) and hence a decreased acquisition time (Figure 2.3b). The number of echoes in each repetition (during the TR interval) is called the Turbo factor.

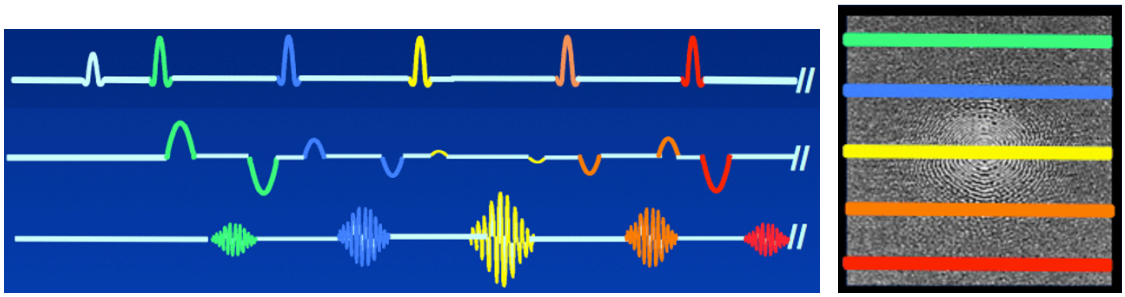

a FSE technique b Corresponding K-space

Figure 2.3: Representation of a Fast Spin Echo Sequence. For each 180° pulse a different phase encoding is applied (a). The resulting MR signals define the filling of the K-space (b), in which each colored line corresponds to the signal collected during the sequence period displayed in the same color. The signals with more information correspond to the center of the K-space. Adapted from [3].

GE sequences are in the category of rapid imaging, like FSE, but differ from SE sequences essentially because no 180° pulses are applied. Since GE sequences only apply RF excitation pulses, bipolar gradients are used to generate echoes. This bipolar gradient is composed of a dephasing gradient followed by a rephasing gradient (Figure 2.4). Usually these sequences are combined with a FA lower than 90° due to the decrease in transverse magnetization that results from it. Thereafter the longitudinal recovery is faster which allows a reduction in TE and TR, decreasing the acquisition time.

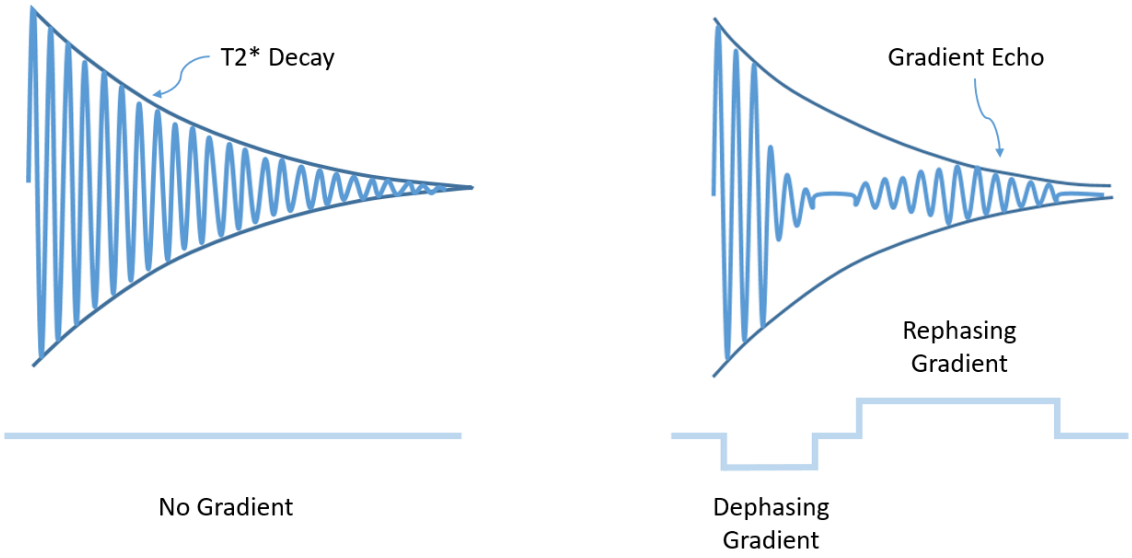

Figure 2.4: Representation of a Gradient Echo Sequence. The application of a RF pulse originates a FID signal, characterized by the time constant T_2^* (left side). By applying a dephasing gradient, an accelaration in dephasing of the spins occurs. This process is then reversed with the application of a rephasing gradient, thus forming a gradient echo (right side). Adapted from [4]

2.1.3 Generating image contrast

Each human body tissue can be characterized by different signal intensities in MRI. These differences between tissues - tissue contrast - can be obtained through means of varying the acquisition parameters, TE and TR. The three most conventional types of image contrast are: T_1-weighted, T_2-weighted and Proton Density (PDn)-weighted.

To acquire a T_1-Weighted Image (WI) it is necessary to use a short/medium TR so that differentiation between longitudinal magnetization of tissues happens and the signals reflect substantially the T_1 values of each tissue. Additionally, TE is related to the transverse relaxation which implies, for this weighted image, using a short TE that suppresses T_2 effects (Figure 2.5). In the case of a 90º pulse application, the interaction of the chosen TR and TE with the resulting longitudinal and transverse magnetization can be observed, respectively, in equations 2.2 and 2.3.

$$M_z = M_o\,(1 - e^{-\frac{TR}{T1}}) \tag{2.2}$$

$$M_{xy} = M_o\, e^{-\frac{TE}{T2}} \tag{2.3}$$

In order to minimize the influence of T_1 on the image, a long TR must be applied. Thus, the longitudinal magnetization of tissue returns to its equilibrium state before the next excitation pulse is applied. This allows the acquisition of a T_2-WI or PDn-WI (Figure 2.5). Therefore, by varying these parameters it is possible to obtain different tissue contrasts and emphasize given structures.

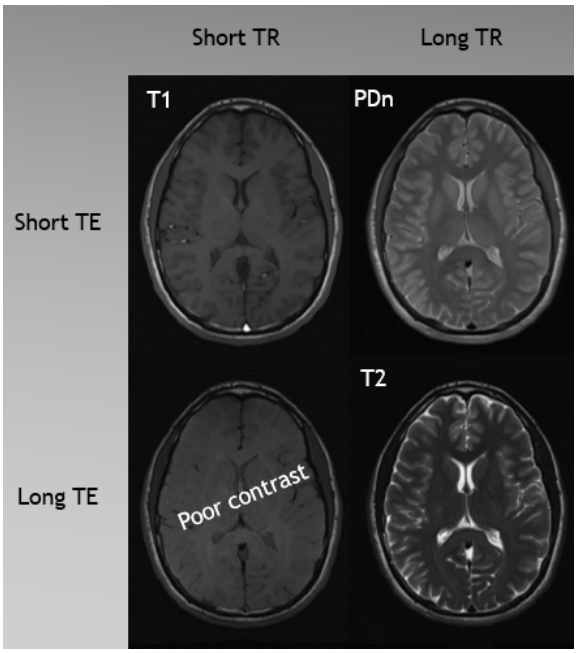

Figure 2.5: Influence of parameters TE and TR on the resulting weighted images. Adapted from [5].

2.1.4 Spatial Resolution and SNR

Good spatial resolution on a MR image is an essential requirement to acquire quantitative anatomic information. Spatial resolution depends on the voxel sizes that in turn are determined by the matrix dimensions, Field of View (FOV) and slice thickness.

The matrix size depends on the number of phase encodings in one direction and the number of frequency encodings on the other direction – perpendicular to each other. Usually, more frequency encodings are applied because it enhances spatial resolution without increasing the acquisition time. The FOV is the area size that the matrix will occupy. Thus, the bigger the FOV, for a given matrix, the worse is the spatial resolution. The slice thickness corresponds to the voxel depth. This is, usually, the biggest dimension

in 2D sequences. Hence, of the three dimensions, slice thickness is the one that presents the worst resolution.

Signal-to-Noise Ratio (SNR) is another measure of image quality and is calculated as the ratio of the mean signal intensity over the standard deviation of the noise. Equation 2.4 shows how SNR is extremely influenced by the selected acquisition parameters of a 2D MRI sequence:

$$SNR = K * (voxel\,volume) * \sqrt{\frac{N_{PE} * NSA}{bandwidth}} \tag{2.4}$$

Where constant K represents the influence of several hardware dependent factors, field strength, pulse sequence type parameters, such as TE and TR, and tissue dependent parameters. N_{PE} is the number of phase encoding steps and NSA (number of signals averaged) represents the number of times that each phase encoding is repeated.

SNR is directly proportional to the field strength. As the field strength increases, there is an increase in the longitudinal magnetization due to the larger number of protons aligned with the B_0 axis. This translates in a signal enhancement for each voxel and, consequently, higher SNR.

By increasing the TR, higher values for the longitudinal magnetization can be reached and, with this, higher SNR. However, it is important to have in mind that high repetition times can be accompanied by a reduction of T_1 effects, altering the contrast. With a lower TE, there is more signal and hence better SNR. Another important parameter that can alter the SNR is the number of averages (NSA) acquired for an image. As the number of averages increases, so does the SNR.

A greater spatial resolution implies a smaller voxel size and with a reduction in voxel size there is less signal from each voxel, resulting in a worse SNR - as it can be observed in equation 2.4. Therefore, when acquiring a MRI there is always a compromise between spatial resolution and SNR.

2.2 Parkinson´s Disease

2.2.1 Pathophysiology of PD

PD affects over 1% of the world population over 55 years old and almost 3% of the population over age 70 [6]. In Europe, PD's crude prevalence rate ranges from 65.6 per 100000 to 12500 per 100000 [7]. PD's etiology is still unknown, even though several studies hypothesized that degeneration is caused by a combination of factors such as ageing, genetic predisposition and environmental factors, such as toxins, infections, mitochondrial dysfunction and oxidative stress [8, 9, 10].

PD is a progressive, neurodegenerative disease that affects the nerve cells of the *pars compacta* portion of the *substantia nigra* (SN) situated in the mesencephalon (Figure 2.6). The SN is divided into two anatomical areas that present distinct functions - *Substantia*

Nigra pars compacta (SNc) and *Substantia Nigra pars reticulata*. However, only the SNc is directly associated with PD [10]. The SNc neurons produce neurotransmitters - dopamine – which are responsible for controlling motor functions. The dopamine is then released by the SNc to the striatum - brain structure that has control over the motor information exchange between the spinal cord and the brain [11]. Another important characteristic of PD is the degeneration of the locus coeruleus (LC), located in the tegmentum of the upper pons. Such results in a reduction of the neurotransmitter norepinephrine on the frontal cortex, hypothalamus and other brain structures [12].

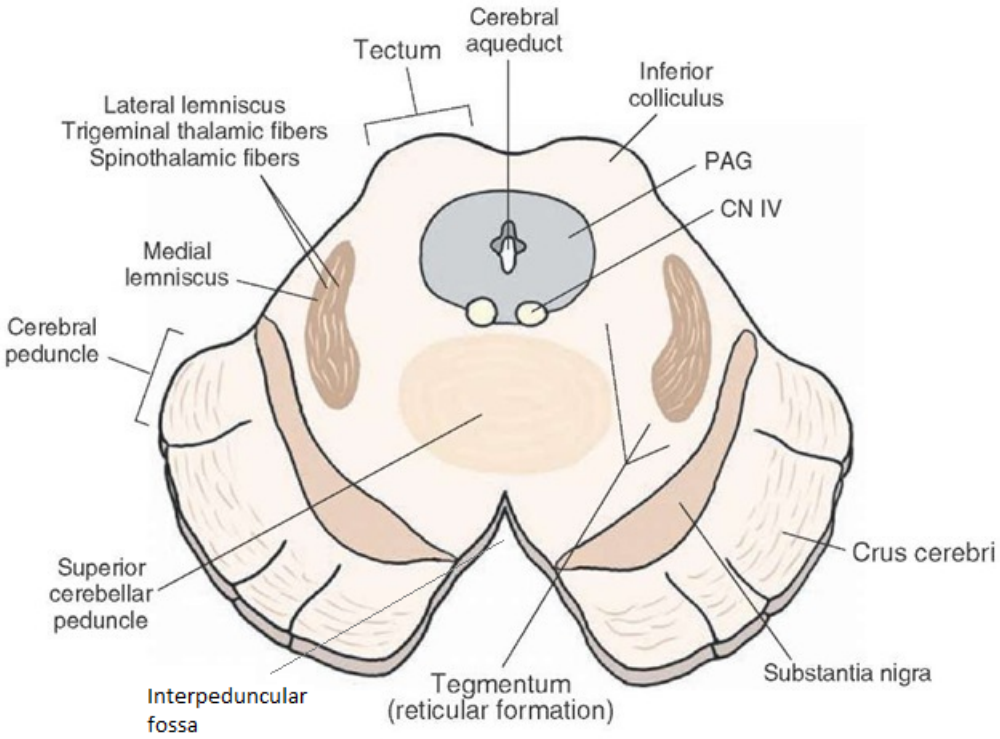

Figure 2.6: Midbrain section of the mesencephalon illustrating relevant structures for this work, such as the *substantia nigra*, the interpeduncular fossa and the decussation of superior cerebellar peduncle. Adapted from [13]

In PD, the SNc neurons suffer a progressive loss resulting in a decrease in the production of dopamine. This leads to a reduction in stimulation of the dopamine receptors localized on the striatum, which in turn can cause secondary effects of mostly enhanced activity of other movement-related brain structures (Figure 2.7). The internal segment of the globus pallidus becomes overactive which can lead to appearance of tremor. The subthalamic nucleus is also hyper-stimulated leading to an inhibitory effect on the thalamus and consequently reduced output to the motor cortex, which explain the symptoms [11, 14]. Only when around 60% to 80% of the nerve cells are depleted, PD symptoms start to manifest [15]. The main symptoms are resting tremor, muscle rigidity, bradykinesia (slowness of spontaneous movement), hypokinesia (diminished range of motion) and postural instability [16].

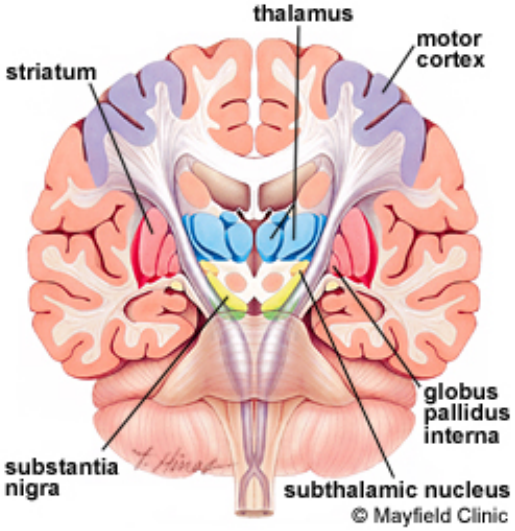

Figure 2.7: Brain anatomy. Brain structures associated with PD: Striatum, *Substantia Nigra*, Thalamus, Subthalamic Nucleus and Globus Pallidus. Adapted from [11]

The Unified Parkinson's Disease Rating Scale (UPDRS) is the most accurate and commonly used rating tool to assess severity and status of PD [17]. The Movement Disorder Society developed this scale, incorporating four main components; Part I evaluates "nonmotor experiences of daily living"; Part II evaluates "motor experiences of daily living"; Part III registers "motor examination" and Part IV concerns "motor complications." For each component, there are several questions that are classified using a scale ranging from 0 (normal) to 4 (severe).

PD is an incurable neurodegenerative disease that has few treatments for the attenuation of symptoms and trying to slow its progression. The most used anti-Parkinson drug is L-dopa, also known as levodopa, which is a natural dopamine precursor [18]. When PD treatment using medication is no longer effective in the reduction of motor complications, recurring to surgery with Deep Brain Stimulation (DBS) is a common procedure.

2.2.2 Neuromelanin

Many studies have revealed that the SNc is constituted by neurons with high concentrations of neuromelanin [19]. This concentration linearly increases with age [20], however in PD patients there is a decrease of NM which is believed to be connected with the dopamine loss (Figure 2.8).

Neuromelanin is a dark insoluble pigment found highly concentrated on dopaminergic neurons of the SNc, confined in cytoplasmic organelles. Additionally, NM has high affinity for metals, particularly iron, and it has been demonstrated that the main neurons who store iron also contain neuromelanin [20]. A few studies have demonstrated that the iron concentration is increased in PD patients [22], possibly as a response to the dysfunctional nigral neurons and consequent iron release. Nevertheless, this topic remains controversial,

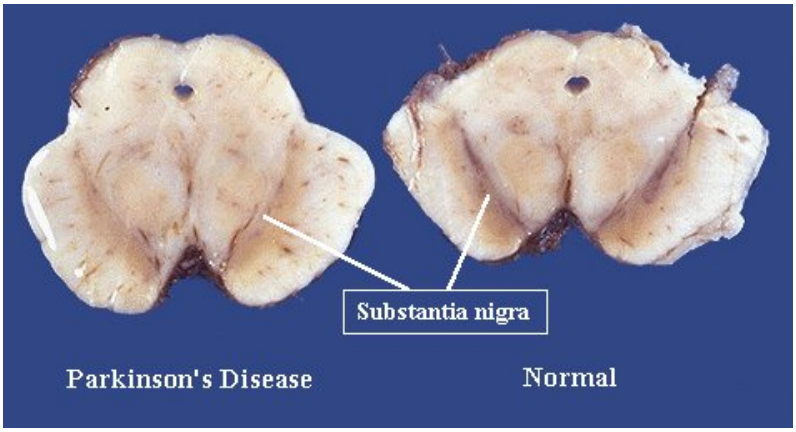

Figure 2.8: Midbrain sections showing the neuronal loss in a PD brain (left) and a healthy subject brain (right). The neuronal loss in the SN of the PD brain can be seen due to the neuromelanin's properties. Adapted from [21]

since other published studies did not find significant differences in iron concentration between PD and controls [23].

Due to its composition, NM seems to have two very distinct roles: protective and toxic. It has a protective function because of its antioxidant properties that defend the cells from redox active metals. However, when the neuromelanin-containing neurons die, NM is released to the surroundings where, due to its insolubility, it stays and can potentially release metals and toxic compounds that may damage other tissues and worsen PD [20].

2.3 Deep Brain Stimulation

2.3.1 Introduction to the technique

DBS is a commonly used treatment for patients with PD [24, 25]. This technique delivers electrical stimulation to deep brain target structures, such as the STN, via electrodes and an Implantable Pulse Generator (IPG) implanted into a subcutaneous pouch in the subclavicular area (Figure 2.9).

It is believed that DBS stimulates axons of the STN, triggering a sequence of events that leads to a dopamine release of the SN neurons. When STN stimulation occurs, either excitatory glutamatergic inputs are sent directly to the SN dopamine cells or excitatory cholinergic/glutamatergic inputs are sent indirectly through the Pedunculopontine Tegmental Nucleus (PPT) to the SN [27] (Figure 2.10). With this, there is an enhancement of dopamine release from the SN neurons to the striatum, motor control is slowly regained and thus an improve in PD symptoms can be achieved [27].

A series of studies have been developed with the aim of exploring DBS effects on PD patients [24, 25], mostly inspired in investigating the safety of these patients with DBS systems implanted.

The DBS system is constituted by electrodes (Figure 2.11), an Implantable Pulse

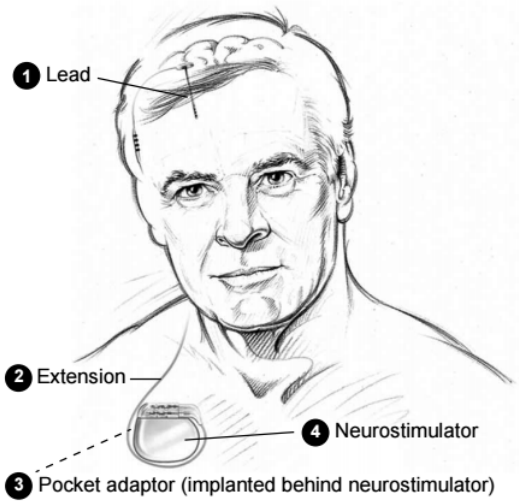

Figure 2.9: Medtronic Deep Brain Stimulation System components. Adapted from [26].

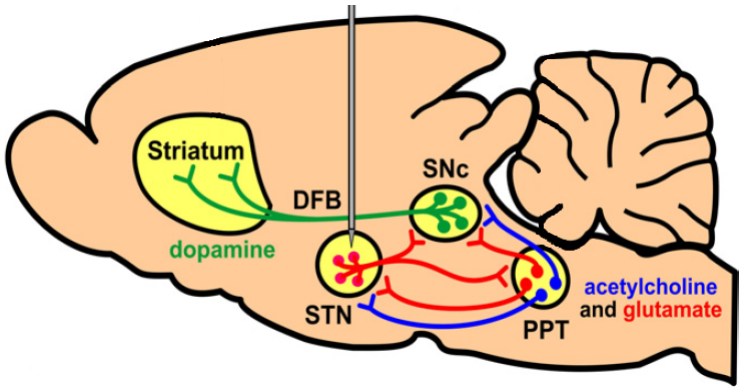

Figure 2.10: Illustration of the STN electrical stimulation showing the effects on PPT and SN, which lead to dopamine release on the striatum. Adapted from [27].

Generator (IPG) and extension cables that connect these components. Each electrode has four metal contacts with neural tissue. When voltage is induced, either through a single contact and the IPG - monopolar stimulation - or between two contiguous contacts - bipolar stimulation -, current is produced and flows to the target tissues [28].

2.3.2 Safety Concerns

The main safety concern with DBS systems in MRI is the sudden increase of temperature on the electrode contacts. This temperature rise results from the effect of the RF pulses applied during the acquisition of the MRI on the DBS system, also known as the antenna effect [29]. The antenna effect suggests that the extended cables used in DBS act as antenna wires, which are sensitive to the electric component, as opposed to the magnetic component of the RF radiation used in MRI. When the electromagnetic waves reach the antenna, they have associated electric charges and consequently currents. When resonance occurs, these currents flow to the tip of the antenna, where the electric energy stays concentrated,

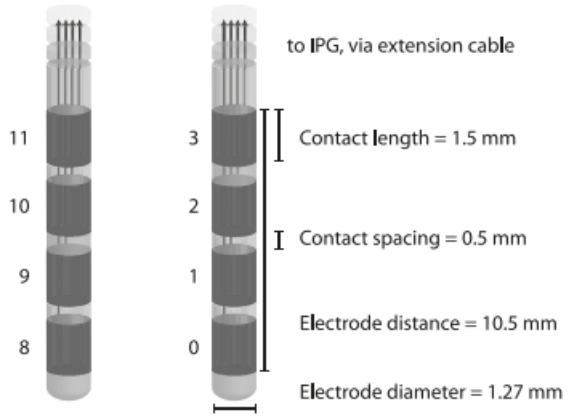

Figure 2.11: The Medtronic 3389 DBS electrodes for bilateral stimulation. Each electrode has four metal contacts spaced between each other. Contacts 0 and 8 are the deepest. The arrows represent the extension cables that connect the electrodes to the IPG. Adapted from [28].

resulting in a localized increase of temperature [30].

Two case studies reported MR Imaging-related accidents in patients with DBS systems implanted [31, 32]. Thus, establishing the safety of performing MRI in patients with subthalamic deep brain stimulators became a priority. Nowadays, safety considerations have to be taken into account when performing MRI scans in patients with neurostimulation systems, namely the impossibility of using 3T MRI systems on these cases [33]. The strong magnetic field characteristic of 3T machines implies an increase of the RF pulses frequency and consequently induces more easily a temperature rise on the tissues, which was demonstrated to be harmful [30]. An evaluation of safety using 1.5T MRI was performed and it was proved that the temperature increase can be controled at said field strength [34]. Since then, numerous 1.5T MRI sequences have been tested confirming that it is safe to obtain these images on patients with implanted neurostimulators [35], as long as a few additional restrictions are obliged.

The most important considerations, in addition to the usage of a 1.5T MRI scan, are: to turn off the DBS stimulation while performing the scan and when defining the parameters for the MRI sequence, the Specific Absorption Rate (SAR) presents a threshold imperative to respect [33]. These limits are described in Table 2.1. The SAR measures the rate at which energy is absorbed by the body. The purpose of this metric is to indirectly evaluate the temperature increase on body tissue, caused by the RF energy deposition [35]. SAR is proportional to the power of 2 of the resonance frequency, as shown in equation 2.5 [36]:

$$SAR \propto B_0^2 * (flip\ angle)^2 * (RF\ duty\ cycle) * (patient\ size) \tag{2.5}$$

Thus, as the frequency of the pulsed RF field increases with the field strength of the magnet, SAR also increases [37]. In order to obtain SAR reduction without changing the field strength, a decrease on the number or amplitude of the RF pulses can be made.

The SAR estimate is, however, dependent on the patient's size and mass and it varies according to the model used by each MRI manufacturer [38]. Therefore, the B_{1+RMS} parameter was recently presented as a more accurate measure of potential implant heating in MRI scanners [39] (Table 2.1). B_{1+RMS} is the time-averaged RF magnetic field component responsible for the creation of an MR image. B_1 is the magnetic field generated with the application of RF pulses, which presents rotating components, the positive one being responsible for the protons flip that generates the MR images. B_{1+RMS} is thus a measure of the magnitude of the positive rotating component of the B_1 magnetic field necessary to create an MRI in 10 seconds [38].

	SAR (W/Kg)		B_{1+RMS} (μT)
	Whole body	Head	
3T	$\leq$2	$\leq$3.2	$\leq$2.8
1.5T with DBS system	$\leq$0.1	$\leq$0.1	$\leq$2

Table 2.1: SAR and B_{1+RMS} maximum values that ensure safe examinations - at 3T and at 1.5T with implanted DBS systems.

2.4 NM-MRI sequence

In 2006, Sasaki et al [40] developed the first MRI sequence capable of identifying *in vivo* neuromelanin-containing structures, namely SN and *locus coeruleus*, from the surrounding brain. The proposed NM-MRI sequence was a T_1-weighted FSE applied at 3T.

The images corresponding to this sequence revealed band-like high signal areas in the posteromedial portion of the cerebral peduncle visualized at the level of the midbrain (Figure 2.12b) [40]. This finding agrees well with the presence of NM in the SN, in *in vivo* slices (Figure 2.12a), suggesting that the NM-containing SN neurons are related to the high-signal intensity. This relation was later confirmed by another study, which noted a clear correlation between the signal intensity and the density of the NM containing neurons, for different parts of the SN [41]. Furthermore, the signal intensity in PD patients was revealed to be reduced in comparison with healthy subjects, in agreement with the progressive loss of SN neurons that occurs on PD patients.

A possible explanation for the obtained contrast is that NM's paramagnetic properties facilitate its orientation with the direction of the external magnetic field, resulting in an acceleration of the T_1 relaxation and thus explaining the high signal intensity of the NM [40]. Additionally, it was suggested that the high iron concentration in the SN may have contributed to the T_1-shortening effects [40]. Although a posterior study found no apparent influence of iron deposition on the signal intensity of the SN [41], the influence of iron in MRI is still not completely understood [43].

Another essential requirement for the correct identification of the SN signal is the choosing of the slice orientation. The sections must be set it the oblique axial plane, oriented perpendicular to the fourth ventricle floor, starting from the inferior border of

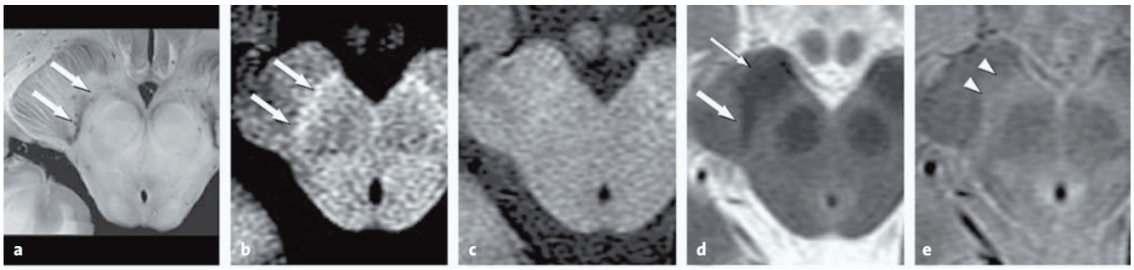

Figure 2.12: Neuromelanin-sensitive and conventional magnetic resonance images of the *substantia nigra*. Axial sections at the level of the midbrain; macroscopic specimen (a) and MR images obtained at 3T with NM-MRI (b), T1-WI (c), T2-WI (d) and PDn-WI (e). The arrows on (a,b) indicate the SNc. On (d) the large arrow points to the SN and the small arrow to peduncular fibers. The arrowheads on (e) point to the SN. Adapted from [42].

the pons to the posterior commissure region [43] (Figure 2.13). The slice orientation in NM-MRI is particularly important due to the small number of slices, three at best, in which the SN is visible. Additionally, in NM-MRI sequences the slice thickness is usually larger than the resolution, which can cause partial volume effects and hence potentially hinder the SN detection. For these reasons, slight alterations in the slice angulation could alter significantly the delineation of the SN in the MR images, emphasizing the importance of choosing a correct slice orientation.

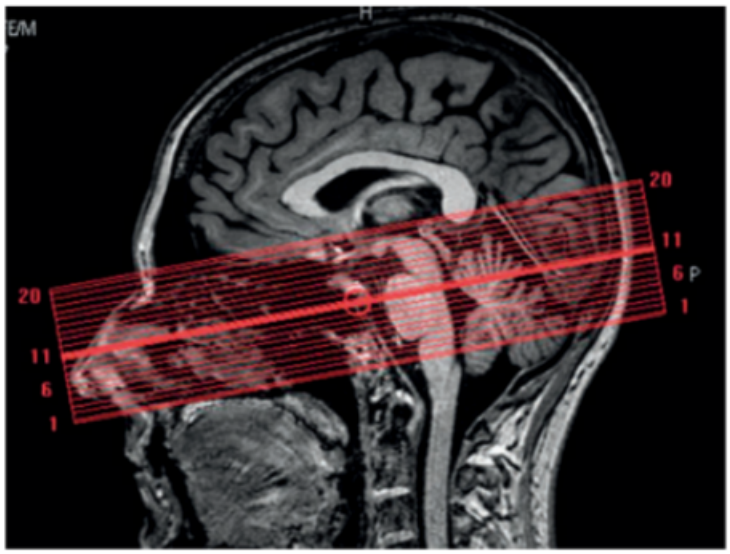

Figure 2.13: Correct slice orientation of a neuromelanin-sensitive MRI sequence. Adapted from [43].

Conventional T_1-weighted SE sequences have failed to capture NM-generated signals (Figure 2.12c). Also, on T_2-WI, the SN region shows low signal intensity and contrast (Figure 2.12d). On a proton density-WI, the *substantia nigra* can be identified as a gray-matter signal area, however the SNc cannot be distinguished from the *substantia nigra*

pars reticularis (Figure 2.12e) [44].

Meanwhile the majority of studies have been applying T_1-weighted FSE sequences at 3T (Table 2.2) with good spatial resolution [45]. The SNR at 3T is twice as higher than at 1.5T and at 3T the relaxation time T_1 of the brain tissue is higher. This implies a signal suppression of the surrounding brain tissue caused by the longer T_1 [46] and, consequently, an enhancement of the neuromelanin-contrast [40]. Additionally, FSE sequences are associated with increased incidental Magnetization Transfer (MT) effects [47]. All these factors contribute to the successful visualization of NM-containing tissues but the key factor is believed to be the MT effects that result from the multiple applications of RF pulses.

MT is a process where spins transfer energy (magnetization) from bound protons to free protons. Usually the MR signal reflects only the magnetization associated to free protons due to their long T1 and T2 values. The bound protons, which have very short T2 values, reach magnetization saturation very quickly. In the case of FSE sequences, the application of multiple 180^{o} pulses facilitates the magnetization saturation of the bound protons leadind to a magnetization transfer to the free protons. With this, a reduction in the MR signal associated to the bound protons occurs, resulting in an enhanced contrast [48].

Recently, a 3D Gradient Echo sequence with an additional MT pre-pulse was proposed for visualizing NM at 1.5T [49] but no subsequent studies have been reported at this field strength. This sequence revealed to have the needed resolution for enabling the observation of SN and *locus coeruleus*. The acquisition parameters of the referred sequence, as well as of previously mentioned related NM-MRI sequences are presented in Table 2.2 for a more easy comparison.

With the GE sequence, the determinant factor for a good achievement of NM contrast was the application of a Slice Selective Off Resonance Sinc (SORS) pulse with Saturation Transfer Contrast (STC), which generates MT contrast. When the surrounding brain tissue signal is suppressed by the STC, the contrast between this tissue and the NM is enhanced, also due to the T_1 reduction caused by the NM and confirming the theory that MT effects are reduced in tissues that contain paramagnetic substances [50]. This study demonstrated that it is possible to visualize NM contrast at 1.5T due to the applied MT pulse. Another study [51] corroborated this theory and showed that GE sequences with MT preparation pulses are able to produce better contrast than FSE sequences, which rely solely on incidental MT effects [52]. Such is consistent with the observation that most NM-MRI contrast is derived from MT effects. In [53], a NM-MRI protocol with a single slice of the SN was tested and it was not possible to distinguish the SN from the surrounding brain tissues, thus corroborating the importance of MT effects in NM-MRI.

MRI sequence		MRI protocol								
		TR (ms)	TE (ms)	Turbo factor	FA (º)	FOV (mm^2)	Pixel size (mm)	Matrix	Slice thickness (mm)	Acquisition time (min:sec)
2D	Sasaki - 3T T1W FSE	600	14	2	90	220×220	0.31×0.36	512×320*	2.5	12
	Schwarz - 3T T1W FSE	688	9	2	90	-	0.47×0.47	-	2.5	12
	Chen - 3T T1W FSE	600	12	2	90	162×200	0.39×0.39	416×512	3	12:34
	Chen - 3T GE	260	2.68	-	40	162×200	0.39×0.39	416×512	3	12:39
3D	Ogisu - 3T T1W FSE	13	2.2	59	20	220×220	0.69×0.93	320×236	1	6:55
	Nakane - 1.5T GE	40	6.8	-	20	200×200	0.62×0.62	320×320	2	8:20

Table 2.2: MRI protocols of several neuromelanin-sensitive MRI sequences. Sasaki et al [40] developed the first NM-MRI using a 3T scanner. Similar sequences have since been developed using 3T MRI systems; Schwarz et al [54] tested a T1-weighted FSE similar to Sasaki's with an inversion recovery pulse; Ogisu et al [55] developed a 3D sequence with a MT pulse. Chen et al [51] compared a T1W FSE sequence similar to the previously described by Sasaki with a GE sequence with an additional MT pulse. Nakane et al [49] developed the first NM-MRI sequence at 1.5T using a 3D GE sequence with a MT pulse. *In this case, the acquisition matrix is presented, whilst the pixel size was calculated with the reconstructed matrix.

2.5 Statistical Tests

2.5.1 Non-parametric Tests

When performing statistical tests, two contradictory hypotheses are stipulated. These statistical hypotheses are conjectures about the distribution of one or more random variables. The first hypothesis, designated as null hypothesis (H_0), assumes that there is no difference between the parameters. The second hypothesis or alternative hypothesis is denoted as H_1 and represents the opposite of H_0 [56].

The goal of a statistical test of an hypothesis is not to determine whether the statement is true or not, but to determine if it is consistent with the observed sample. As so, the null hypothesis should only be rejected when the observed data has a very low probability of being true. By defining a *p-value* lower than 0.05 as significant, if the obtained result is indeed significant ($p < 0.05$) the null hypothesis is rejected. Otherwise, if ($p \geq 0.05$), H_0 is supported [56].

There are two main statistical tests: parametric and non-parametric tests. Non-parametric tests are applied when no assumptions that the data is influenced from a given probability distribution are made, as opposed to parametric tests. Non-parametric tests are usually used in cases with small samples (n $<$ 30), also these are more accurate than parametric tests when the normality of the data cannot be assumed [57].

For these reasons, in the present study, the following non-parametric methods were applied: Friedman test and Wilcoxon signed rank test.

The Friedman test is used to test for differences between three or more related groups, where the hypotheses to be tested are [58]:

- H_0: All groups came from the same population or from populations with the same distribution;
- H_1: Not all groups have the same distribution.

The Wilcoxon signed rank test is used to compare paired samples. The samples must be dependent within the par (paired samples) and independent between pairs [59]. The tested hypotheses of the Wilcoxon test are:

- H_0: The median difference between paired samples is zero;
- H_1: The true location shift is not equal to zero.

2.5.2 Intraclass Correlation Coefficient

For any measurement procedure to be used in clinic practice, reliability of the method has to be established. The chosen method for analyzing test-retest reliability of the semi-automatic algorithm is the Intraclass Correlation Coefficient (ICC). This is the only

measure of reliability that measures both correlation and agreement between measurements [60].

The ICC can assume different forms according with the type of study that is being performed. Its values always range from 0 to 1, with values closer to 1 representing stronger reliability. As in the present study test-retest reliability is being assessed, ICC estimates and their 95% confidence intervals were calculated based on a single measurement, absolute agreement, 2-way mixed-effects model, as defined by McGraw and Wong [61].

2.5.3 Bland-Altman Method

In this study, the agreement between two methods of measurement - SN areas taken with the 1.5T sequence and with the 3T sequence - had to be assessed. To do so, the graphic statistical procedure proposed in 1983 by Altman and Bland [62] was performed. This method evaluates the agreement between two quantitative measurements by calculating the mean difference and limits of agreement of the said measurements.

The resulting graphic is a scatter plot XY, considering that the obtained measurements from the two different methods are represented by the variables A and B, in which the Y axis represents the difference between the paired measurements and the X axis the average of those measures (Figure 2.14). The Bland-Altman plot has a confidence interval of 95 %, meaning that 95 % of the data should lie within $\pm 1.96SD$ (standard deviation) of the mean difference. The bias is represented by the gap between the mean difference of two measurements and the X axis, which corresponds to zero differences [63].

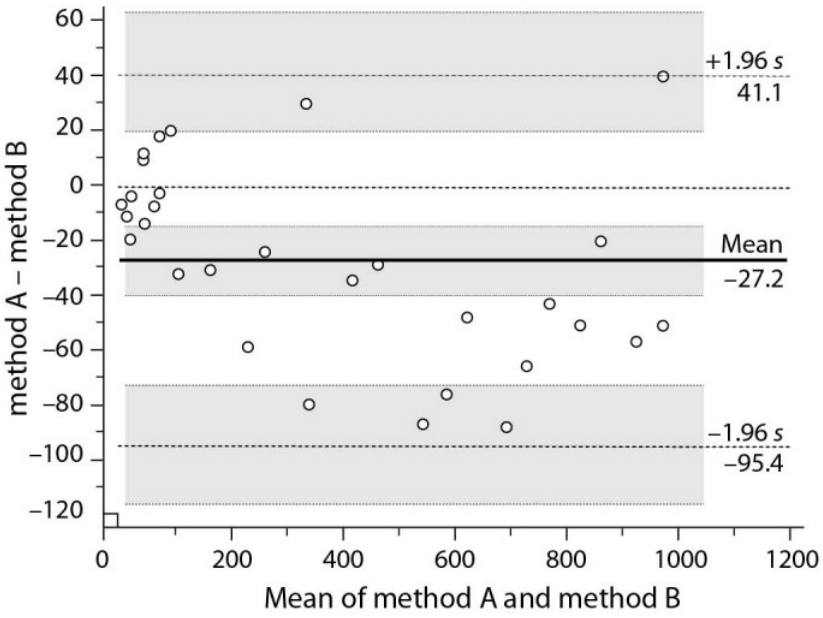

Figure 2.14: Example of a Bland-Altman plot of differences between method A and B *Vs.* the mean of the two measurements. The bias and the confidence interval limits are also represented. Adapted from [63].

While other agreement analyses, such as the ICC, have defined criteria to evaluate the level of agreement between measurements, the Bland-Altman method only provides the intervals of agreement and it us up to the user to interpret whether those limits are acceptable or not.

CHAPTER 3

Validation of a 1.5T NM-MRI sequence

Neuromelanin-sensitive MRI is a promising technique to allow the visalization *in vivo* of the pathological changes in NM-containing structures that occur in degenerative disorders and has recently also been applied to psychiatric disorders [42]. The majority of studies have applied NM-MRI at 3T due to its improved resolution and SNR. However, availability and safety reasons due to patients with implantable devices such as neurostimulators, cardiac pacemakers and cardioverter-defibrillators may prevent imaging at this field strength [64, 65]. This chapter describes the development of a 1.5T NM-MRI sequence through adaptation of the commonly used 3T NM-MRI sequence in clinic practice. These two sequences were compared using a semi-automatic segmentation algorithm applied to the SN, aiming to establish the feasibility of the developed 1.5T sequence. Additionally, differences in the contrast ratio of the tested sequences were assessed.

3.1 Materials and Methods

3.1.1 Sample Description

Twelve individuals (4 males and 8 females), with ages ranging from 38 to 85 years (mean age: 62.5 ± 13.1 years) were included in the present study. From this pool, seven subjects were diagnosed with PD by a movement disorders specialist according to the PD UK Brain Bank criteria [66]. The remaining five subjects had still an undetermined diagnosis but presented movement-related disorders. Patients were recruited from the Movement Disorders Unit of Hospital of Santa Maria-Lisbon.

All subjects provided informed consent for the examinations performed on this study.

3.1.2 Imaging Protocol

To develop a 1.5T NM-MRI applicable in clinic practice and with an adequate reproducibility and image contrast, the 3T T_1-weighted FSE sequence currently used at Hospital of Santa Maria-Lisbon was the starting point from which the 1.5T sequence was adapted from. The necessary changes are discussed next in subsection 3.1.2.1.

The 3T sequence had the following acquisition parameters: repetition time/echo time of 606/10ms; turbo factor of 3; FOV of 220×190 mm^2; matrix size of 548×474 (pixel size of 0.40×0.40 mm^2); slice thickness of 2.5mm with no gap; four averages; Parallel Imaging (PI) with reduction factor of 1.5 and an acquisition time of 8:35 min.

The acquisition parameters of the 1.5T sequence were: TR/TE of 600/10ms; turbo factor of 3; FOV of 220×180 mm^2; matrix size of 440×361 (pixel size of 0.50×0.50 mm^2); slice thickness of 2.5mm with no gap; four averages; no PI acceleration, and an acquisition time of 9:45 min.

Both systems used T_1–weighted FSE sequences and all images were acquired with an 8-channel SENSE head coil. All data were acquired with a 3T MRI (Achieva 3.0, Philips Medical Systems, Best, Netherlands) and a 1.5T MRI systems (Intera 1.5, Philips Medical Systems, Best, Netherlands). Each subject underwent a single scan in each MRI system with both acquisitions being performed on the same day, by a random order according to the availability.

In both cases, the sections were carefully set in the oblique axial plane perpendicular to the floor of the fourth ventricle, starting from the posterior commissure to the inferior border of the pons.

3.1.2.1 Analysis of the acquisition parameters

The changes applied to the original sequence were made with the purpose of ensuring sufficient resolution on the 1.5T sequence to enable the visualization of the SN. Adding to this, an effort to change as few parameters as possible was made so that at the time of the analysis, variability sources will have been reduced.

In order to compensate the reduced SNR typical of 1.5T images, the size of the acquisition matrix was reduced, leading to a slightly coarser pixel size (0.5x0.5 mm^2) and consequently a smaller spatial resolution was obtained. The FOV was slightly decreased, although it was not significant so that it would change spatial resolution. These slight changes in the FOV values are very common in the clinic considering that this parameter has to be adjusted according to the head size of each individual patient.

Despite the potential change on T1 contrast due to the alteration of field strengths, TR and TE were kept along the same values, as we expected the intrinsic MT effects to be dominant. The time of repetition was slightly reduced. Nevertheless, this reduction did not have much of an impact on the acquisition time due to the deactivation of SENSitivity Encoding (SENSE).

SENSE is a parallel imaging technique that enables the reduction of the number of phase encoding steps and reconstructs the missing data taking into account the coil sensitivity variation between channels [67], thus enabling a shorter acquisition scan (8:35 min). However, the reduced image information necessary to obtain a shorter scan time results in a diminished SNR related to the reduction factor:

$$SNR_{PI} = \frac{SNR}{\sqrt{R}} \tag{3.1}$$

, where R represents the reduction factor by which the number of k-space samples is reduced. Therefore, considering that 1.5T sequences predictably present a worse SNR when compared to 3T sequences, parallel imaging was not applied to the developed 1.5T sequence and its acquisition time increased (9:45).

3.1.3 Imaging Analysis

Image processing was performed using the OsiriX program (Version Lite) [68]. This program combines visualization features of medical images with various processing tools and is more easily applicable in clinic practice than similar implemented processing in Matlab.

To assess if the developed 1.5T NM-sequence is effective and comparable to the already existing 3T NM-sensitive MRI sequence, as well as able to detect changes in the neuromelanin-containing structures, it is essential to define a method that allows quantitative measurement of the SN.

There have been several reports [51, 55, 69] of SN quantification with different segmentation methods. Most of these studies used two-dimensional (2D) sequences. However, there were divergences regarding the type of SN measurements – area [54, 69] or volume [51, 70]. Since 2D segmentation of a single slice is simpler and faster and therefore more easily included in clinic practice, the SN quantification in this study was made through measurements of the SN area from a single slice. Additionally, the thick slices used in the study (2.5mm) that are necessary to ensure sufficient SNR, can lead to partial volume effects thus originating subjective SN volume measurements.

Once the type of SN measurement is defined, there are two possible segmentation methods – manual or automated. In the present study, a semi-automated segmentation method optimized in a previous Master Thesis [71] was applied. Furthermore, in order to evaluate the repeatability and feasibility of the algorithm, manual segmentation of the SN was used as gold standard. All the segmentation process is described next in subsection 3.1.3.1.

3.1.3.1 Segmentation method

The NM hyper intense signal is typically visible in three slices (Figure 3.1). The middle slice - 3.1b, which presents the largest SN area, was chosen for measurements. In two cases

there were doubts in slice selection owing to the fact that the NM-SN area was visible on more than three slices. For these two subjects only, slices that were visually similar at 1.5T and 3T were chosen.

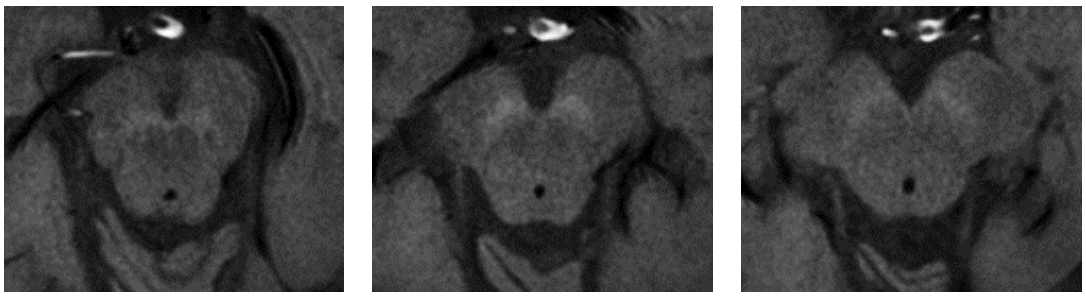

a Lower midbrain b Center midbrain c Upper midbrain

Figure 3.1: Axial sections at different levels of the midbrain showing the *substantia nigra* as a hyper intense signal area. The middle slice (b) was the one chosen for SN measurements.

In order to compensate for the reduced SNR present in NM-MRI that can have an effect on segmentation, a *Guassian blur* filter, which is incorporated in the OsiriX features, was applied to the selected slice (Figure 3.2b).

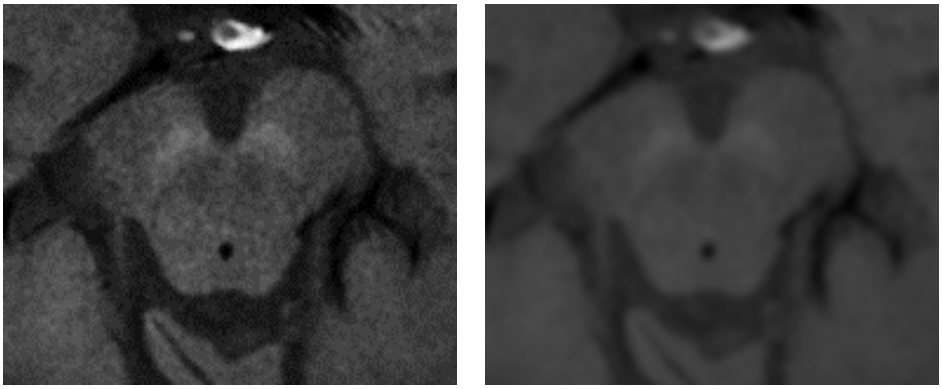

a Original image b Filtered image

Figure 3.2: Selected axial middle slice for SN measurements before (a) and after (b) the application of the *Gaussian blur* filter, showing a clear blur effect of the applied filter.

The *Guassian blur* filter uses a Gaussian function to calculate the kernel (Figure 3.3) that will be applied to each image pixel. During the image convolution, the pixel that is being analyzed is given the highest weight – corresponding to the center pixel of the mask, whilst the neighboring pixels which are covered by the mask, are given increasingly lower weights as the distance between them and the main pixel increases. This filter is commonly used in image pre-processing because it reduces the noise in the image, thus facilitating the segmentation that follows. Additionally, compared to the other filter types already implemented within Osirix, the Gaussian blur filter was demonstrated in [71] to have the best performance in the SN segmentation. The used filter has a kernel dimension

of 5×5 pixels and a Full Width at Half Maximum (FWHM) of 2 pixels.

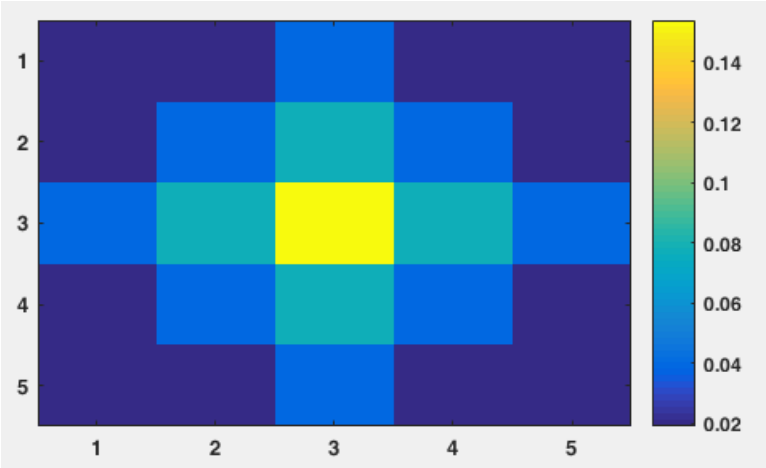

Figure 3.3: Representation of the colored image corresponding to the 5x5 Gaussian blur kernel. The color-bar on the right shows how the data values correspond to the image, with the highest weight being given to the center pixel.

With the selected filtered image displayed, there are some adjustments that need to be done before the application of the segmentation algorithm. The OsiriX software enables to modify the displayed contrast, thereby facilitating the user in visualizing the SN area, as well as zooming in and rotating the image - all helpful tools for the correct identification of the *substantia nigra*.

The OsiriX 2D semi-automatic segmentation tool has three available algorithms: *Threshold*, *Neighborhood* and *Confidence*. This last algorithm was chosen as it was shown in [71] to be the most practical and efficient method for segmentation of the NM-corresponding area. The *Confidence* algorithm requires the definition of three parameters, which define the inclusion criteria: multiplier, number of iterations and initial radius, whose corresponding values for the correct identification of the SN were, as defined in [71] - 2,2 and 1, respectively (Figure 3.4).

The *Confidence* algorithm is based on a commonly used segmentation technique – *Region growing*. This technique enables growth of regions that were previously marked with *seed regions*. That is, starting with the initial selected set of pixels, the neighboring pixels are posteriorly evaluated based on the inclusion criteria to decide whether they should be included in the segmented region or not.

Owing to the fact that the algorithm is based on *Region growing*, the relevance of developing sequences that successfully depict the neuromelanin-containing structures and optimizing image contrast is particularly relevant. A possible source of concern is the placing of the *seed region*, which influences the identification of the Region-of-Interest (ROI). Thus, to minimize the seed placing error and consequent variability of the ROI, a straight line crossing the interpeduncular fossa was drawn (Figure 3.5a), just like it was done in [71]. Along the referred line the SN voxel with the most hyper intense signal was chosen.

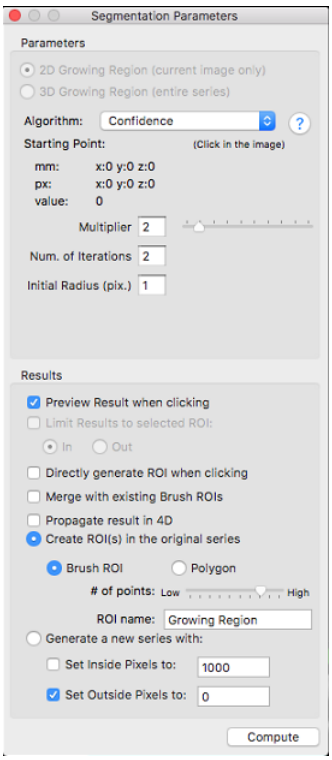

Figure 3.4: OsiriX segmentation tool interface that enables the definition of the segmentation algorithm and respective parameters. In this study, the chosen segmentation algorithm was *Confidence* and its parameters were 2 - Multiplier, 2 - Number of Iterations and 1 - Initial Radius.

After the application of the semi-automatic algorithm, it was common for the segmented SN regions to present gaps (Figure 3.5b). Yet, anatomic examinations have shown that the SN is a structure which does not present gaps. For this reason, a last filter - *Brush closing* - was applied and with this, the gaps that were not being accounted for the area calculation became filled (Figure 3.5c). Finally, with the semi-automatic SN region correctly delineated, the corresponding ROI was saved as well as some of its characteristics, such as area and mean signal intensity, which are available in the OsiriX software.

SN segmentation using the semi-automatic tool explained above was performed three times for each side of the brain in order to assess test-retest reliability. The three repeated measures of the SN ROIs were performed on different days to avoid biasing.

The left and right ROIs of each image were considered independent regions, as it is common in PD for one side to present a more accentuated loss of dopaminergic neurons of the SN, making a total of 24 SN regions to be studied. For each SN region, manual segmentation was also performed on a different day. The SN manual contours were made resorting to an OsiriX tool that enables the user to freely draw over the image, in order to obtain the sought segmented region, and adjust the said region if needed (Figure 3.6). The manual ROIs were all validated by a certified neuroradiologist (Dr. Sofia Reimão) and saved to be used as gold standard.

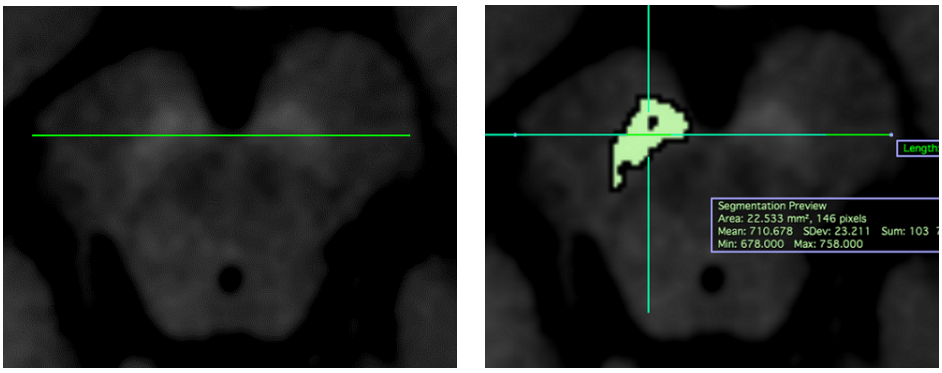

a Pre-segmentation

b *Confidence* algorithm

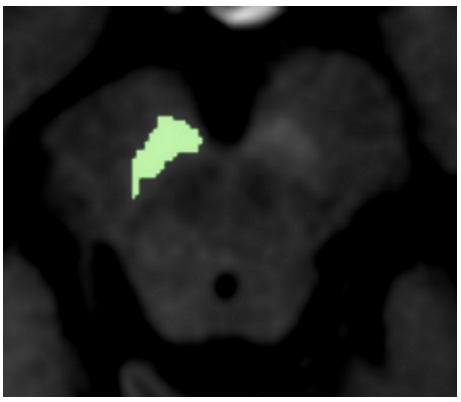

c After *Brush closing*

Figure 3.5: SN semi-automatic segmentation process. First a line is drawn crossing the interpeduncular fossa (a). Then, a pixel along the line is chosen and the *Confidence* algorithm generates the region-of-interest accordingly (b). At last, the *Brush closing* filter is applied to ensure that the selected SN area is completely filled (c).

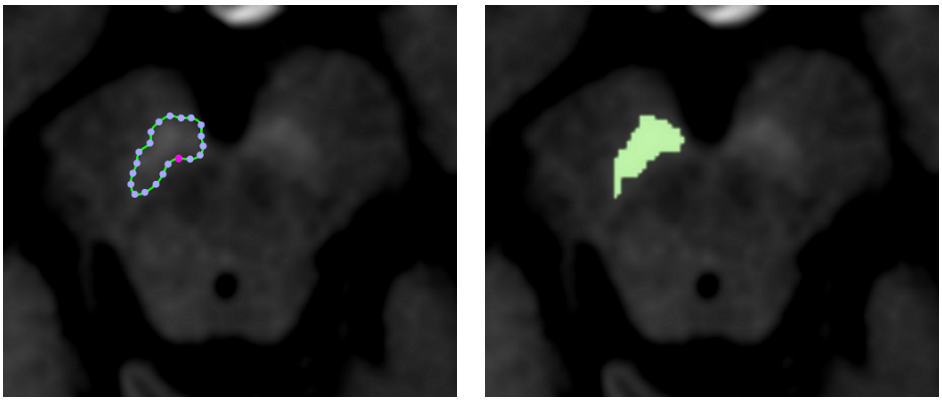

a Manual segmentation

b Semi-automated segmentation

Figure 3.6: Example of the application of a manual (a) and semi-automated (b) segmentation of the SN region on a neuromelanin-sensitive MR image, using the OsiriX software.

3.1.3.2 Similarity Analysis

The analysis of the SN areas is very effective to evaluate quantitative differences in the dimensions of the ROIs, thus enabling the assessment of neuropathological changes. Nevertheless, there is no information regarding spatial distribution of the SN segmented regions.

A very common method used in medical images to assess the reproducibility of segmented regions is the Dice Similarity Coefficient (DSC) calculation [70, 72]. This coefficient quantitatively measures the spatial overlap between two segmented regions, complementing the analysis of the comparison between SN regions.

In this study, the overlap between the semi-automatic SN ROI and the reference manual segmentation was determined using the DSC:

$$DSC = 2\frac{area(SN_{sa} \cap SN_m)}{area(SN_{sa}) + area(SN_m)} \tag{3.2}$$

where area(SN_{sa}) and area(SN_m) represent SN areas for a semi-automatic ROI and corresponding manually-segmented region, respectively, and $\cap$ represents the intersection operator. The DSC ranges from 0, where the segmented regions do not intersect at all to 1, which indicates exact overlap.

An application in Matlab (R2016, The Math Works, Natick, MA, USA) was created to estimate the DSC. The developed interface (Appendix A.1) enables the loading and visualization of two DICOM images, the visualization of the two segmented regions overlap with two possibilities – just showing the region that resulted from the overlap (Figure 3.7c) or displaying the two initial regions and its overlap in different intensities (Figure 3.7d) - and calculates the DSC. Additionally, the application allows the user to zoom in and out on all images and to save the resulting image.

The two DICOM images that were compared with the Matlab application contained a semi-automatic SN region and the other its corresponding manual segmentation. For the application to work, these images had to be taken from the OsiriX program displaying solely the isolated segmented regions. Considering this, the developed script treats the image as binary and assigns the value 1 (white) to every pixel that does not have intensity 0 (black), displaying the region-of-interest as white and the surroundings as black (Figures 3.7a and 3.7b).

3.1.3.3 Image contrast Analysis

FSE NM-MRI sequences rely solely on incidental MT effects to distinguish the NM-containing structures. Furthermore, image contrast at 1.5T is expected to be diminished when compared to 3T. Considering this, it is imperative to evaluate the obtained NM-related contrast in order to assess the feasibility of the 1.5T FSE sequence that is being tested.

Because SN segmentation is performed after application of the *Gaussian blur* filter - the first step of the segmentation pipeline – described previously in 3.1.3.1, it would

a Binarized semi-automated region

b Binarized manual segmented region

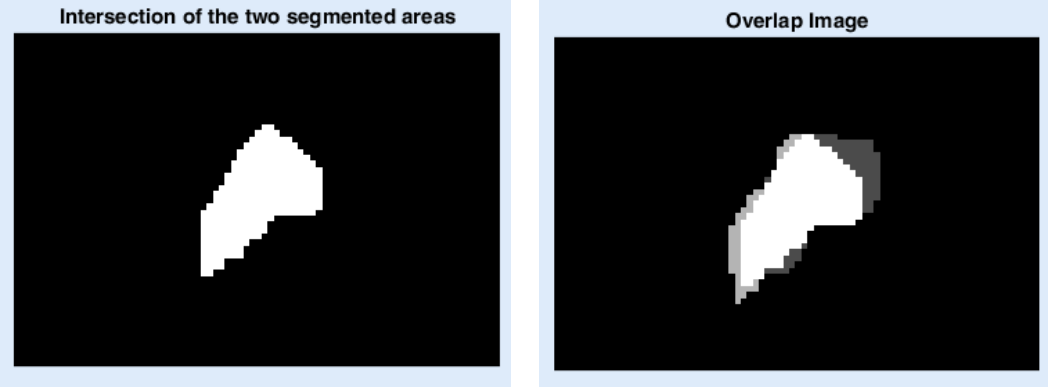

c Binarized overlap region

d Two segmented regions and its overlap

Figure 3.7: Segmented regions after binarization (a,b) and two available display options for visualizing the resulting overlap (c,d) - with the Matlab application for DSC calculation.

be interesting to assess Contrast Ratio (CR) differences between field strengths after the filter application. However, knowing that image filtering may potentially affect the contrast, it is also necessary to evaluate the significance of these differences. Thereby, CR was measured both before and after the filter application, keeping the used ROIs in the exact same positions. Additionally, in order to assess whether differences in CR affect the segmentation, CR was calculated on the same slices that were used to measure the SN areas – for both field strengths.

To evaluate the CR, the fraction I_{SN}/I_{DP} was calculated where I_{SN} represents the mean signal intensity of two 6.0 mm^2 square ROIs (one for each side of the brain) located in the SN portion matching an imaginary line crossing the interpeduncular fossa. I_{DP} is the mean signal intensity of the decussation of the superior cerebellar peduncles determined using a circular reference ROI (diameter of 4.0 mm) (Figure 3.8). The mean signal intensities were measured with OsiriX.

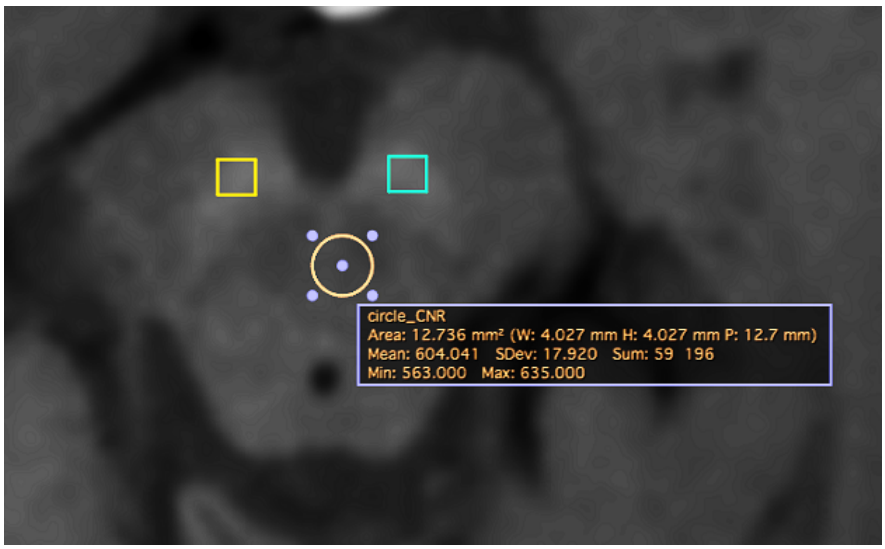

Figure 3.8: Example of a NM-MR image, after the application of a *Gaussian blur* filter, with two square ROIs in the SN and a circular reference ROI located in the decussation of the superior cerebellar peduncles. The mean signal intensities of the ROIs, needed for the contrast ratio calculation, are displayed by the OsiriX software.

3.1.4 Statistical Analysis

All statistical analyses were performed with the R software, version 3.3.3. (R Foundation for Statistical Computing, Vienna, Austria), and a *p-value* lower than 0.05 was considered significant.

For each subject, semi-automatic repeated measurements (area and DSC) were obtained at three different times for each magnetic field strength. The Friedman test (2.5.1 was applied for within-subject comparisons of these measurements. As will be shown later (Section 3.2), since no differences were observed between repetitions, the Wilcoxon signed rank test (2.5.1) was then performed to evaluate pair-wise comparisons between the first semi-automatic area estimate and the corresponding manual area. Both analyses consist of non-parametric tests.

To assess the reliability of the semi-automatic SN measures (area and DSC), a two-way random ICC evaluating absolute agreement (2.5.2) was tested. This coefficient and its 95% Confidence Intervals (CI) were calculated for all subjects and for each magnetic field scanner. The ICC values were interpreted according to the criteria set by Landis and Koch [73] that considers an ICC of (0.8 - 1) as an almost perfect agreement between groups and (0.6 - 0.8) as substantial agreement.

The agreement between SN areas obtained at the two different magnetic fields – 1.5T and 3.0T - was assessed by using the Wilcoxon signed rank test and the Bland-Altman method (2.5.3).

Lastly, the Wilcoxon test was also used to investigate CR differences measured before and after the filter application, to assess whether pre-processing influences significantly the CR values. The comparison of the SN contrast ratio obtained at 1.5T and 3T was also

performed using the Wilcoxon test, both prior to the filtering and following it.

3.2 Results

No significant differences were observed with the Friedman test for either field strengths when comparing between the three repeated estimates of the SN area (Table 3.1). Nevertheless, a higher p-value was obtained at 3T (p=0.9893) than at 1.5T (p=0.5308), as it was expected. The Friedman test applied to the DSC of the different samples of the semi-automatic SN ROIs also revealed no significant differences between the samples for 1.5T (p=0.9892) or 3T (p=0.2430) – Table 3.1.

Although the Friedman tests proved that there were no significant differences in size and spatial distribution between the repeated semi-automatic measures for both field strengths, the repeatability of the algorithm still needed to be assessed. To that end, the intraclass correlation coefficients were calculated for area and DSC at 1.5T and 3T.

The ICC and CI for the SN areas estimated with the semi-automatic algorithm using 1.5T and 3T images are also shown in Table 3.1. A high ICC was obtained in both cases. The SN areas measured at 3T, have an almost perfect agreement between the repeated measures (ICC_{Area}, 3T: 0.913, p<0.001) with a very narrow CI for all ROIs. The agreement of the SN areas estimated from 1.5T images was considered substantial to almost perfect with a wider CI, but a large ICC value (ICC_{Area}, 1.5T: 0.815, p<0.001).

The ICC for the DSC measurements (Table 3.1) indicated substantial agreement, with a wide CI, for both magnetic fields. At 3T the ICC revealed a substantial agreement (ICC_{DSC}, 3T: 0.777, p<0.001). The DSC agreement within the semi-automatic ROI estimated from 1.5T images was almost perfect (ICC_{DSC}, 1.5T: 0.817, p<0.001).

The segmented SN areas estimated with the semi-automatic algorithm (Figure 3.9) showed excellent test-retest reproducibility and revealed good overlap with the corresponding manual segmentations (Figure 3.10). The mean DSC considering the three repetitions was 0.72 [0.67-0.78] (median; [Q1-Q3]) for 1.5T and 0.77 [0.72-0.81] for 3T. According to the criteria defined in [74], the DSC obtained at 3T was excellent (>0.75) and at 1.5T can be considered as good overlap (0.6-0.75). Once again the measurements at 3T showed better results than at 1.5T, as expected.

Considering the excellent reproducibility of the semi-automatic segmentation algorithm, only the first SN areas taken with the algorithm were considered in the remaining analyses. No significant differences were detected when comparing the first semi-automatic and corresponding manually determined SN areas using the Wilcoxon pair-wised comparison, either at 1.5 T (p-value=0.1747) or 3.0T (p-value=0.0574). These results corroborate that the semi-automatic segmentation results are reproducible in images acquired with both magnetic fields and that the SN measures are valid to be used as these were not significantly different from the gold standard (manual measurements).

The analysis with Bland-Altman plot for the SN areas showed good agreement between the semi-automatic measurements obtained at different magnetic fields (Figure 3.11) with a

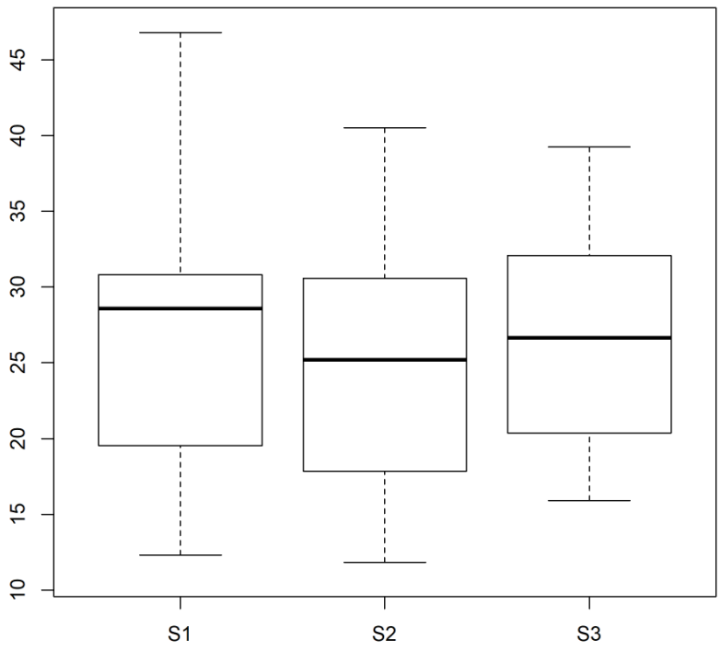

a Plot of SN areas at 1.5T

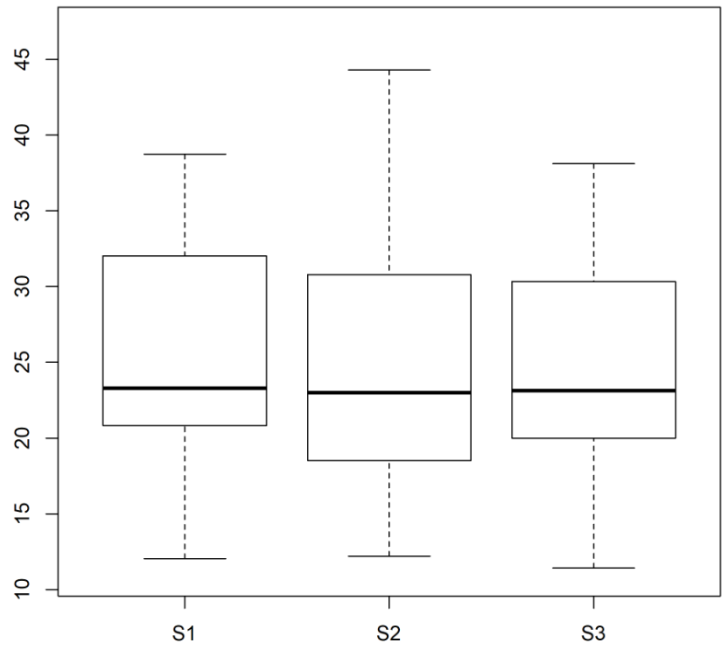

b Plot of SN areas at 3T

Figure 3.9: Box and whisker plot of SN areas (mm^2) estimated with the semi-automatic algorithm (three repeats represented by S1, S2 and S3) for 1.5T (a) and 3T (b).

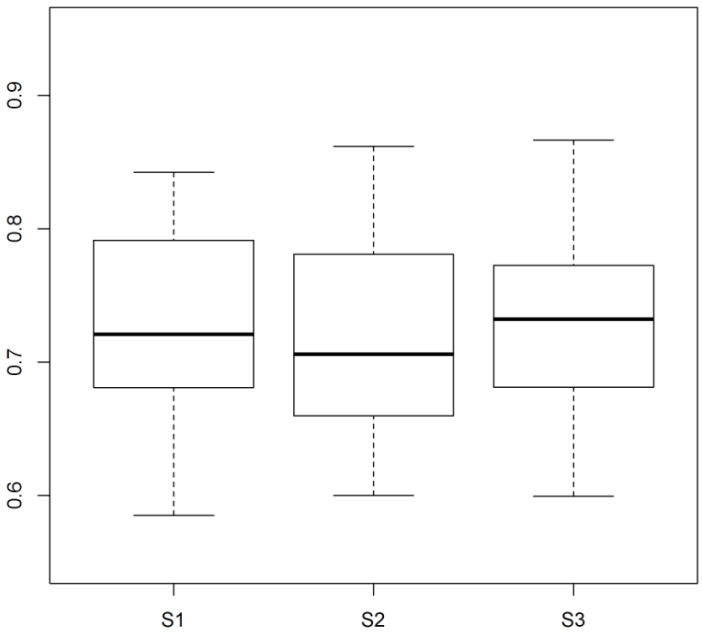

a Plot of DSC at 1.5T

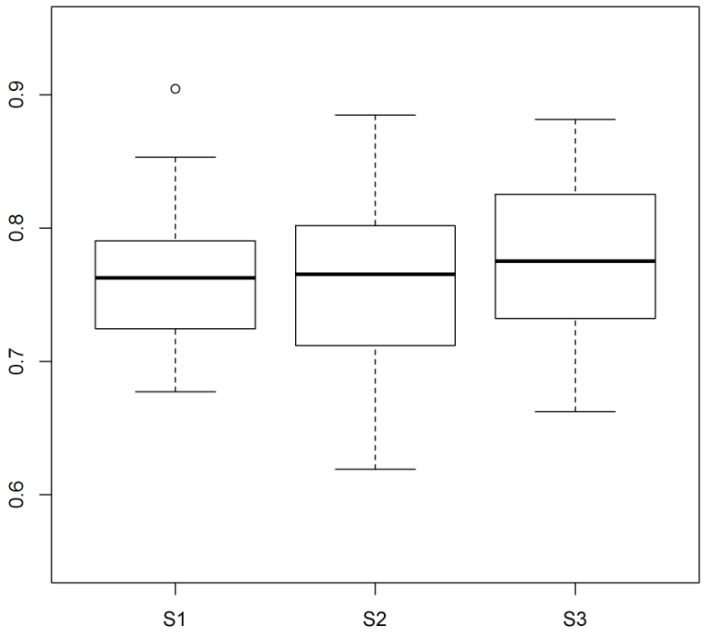

b Plot of DSC at 3T

Figure 3.10: Box and whisker plot of DSC representing overlap between the segmented SN areas, estimated with the semi-automatic algorithm (three repeats represented by S1, S2 and S3) and the manual ROI for 1.5T (a) and 3T (b).

small positive bias of 1.56 mm^2. However, its limits of agreement ranged from -13.07 mm^2 to 16.2 mm^2, which can be considered as a relatively wide range. Since the Bland-Altman results were not conclusive on their own, the Wilcoxon test comparing the same areas was performed and confirmed that the SN ROI estimated from the images collected at different magnetic fields were not significantly different (p-value=0.3596).

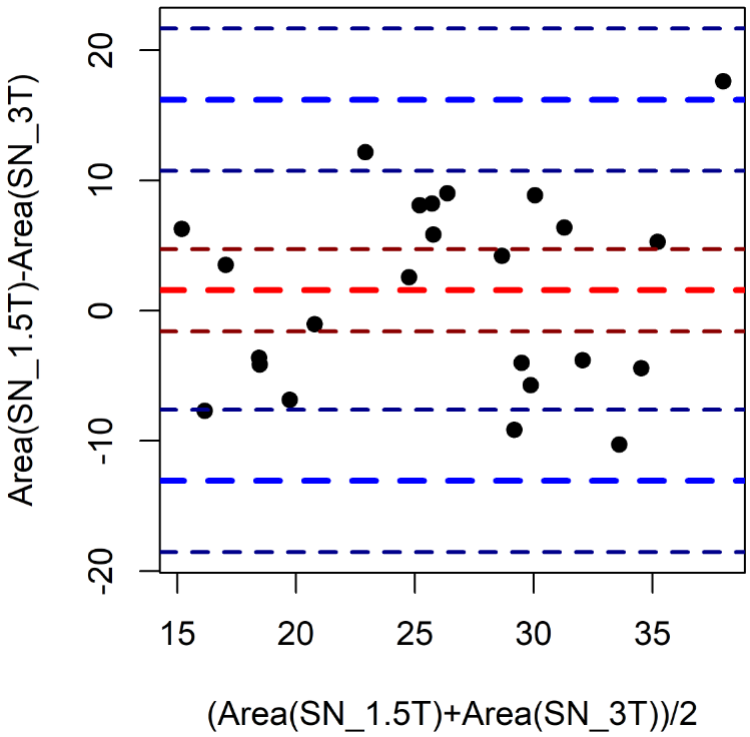

Figure 3.11: Agreement analysis of SN areas between the two different sequences – 1.5T and 3T. The plot shows a bias between the mean differences of 1.56 mm^2 and an agreement interval ranging from -13.07 mm^2 to 16.2 mm^2, with a 95% confidence interval.

When comparing the corresponding CRs calculated before and after the filter application, the Wilcoxon test revealed a really marked significant difference between CRs (p-$value$<0.0001). To evaluate differences between the images obtained at different magnetic fields, the statistical Wilcoxon test was applied to compare the CR measures. This test showed no significant differences between CR values, both before the filter application (p-$value$=0.0640) and after (p-$value$=0.0523), although both values are very small. The distribution of CR values in the SN evaluated at 1.5T and 3T, for both studied cases were also observed (Figure 3.12) and are very similar. The median CR, before image filtering was applied, at 1.5T (1.177) was lower than at 3T (1.205), as expected, and the range at 1.5T [1.141 – 1.223] narrower than at 3T [1.118 – 1.316]. The median CR, after the filter application, at 1.5T (1.163) was lower than at 3T (1.193) and the range at 1.5T [1.135 – 1.200] narrower than at 3T [1.123 – 1.303].

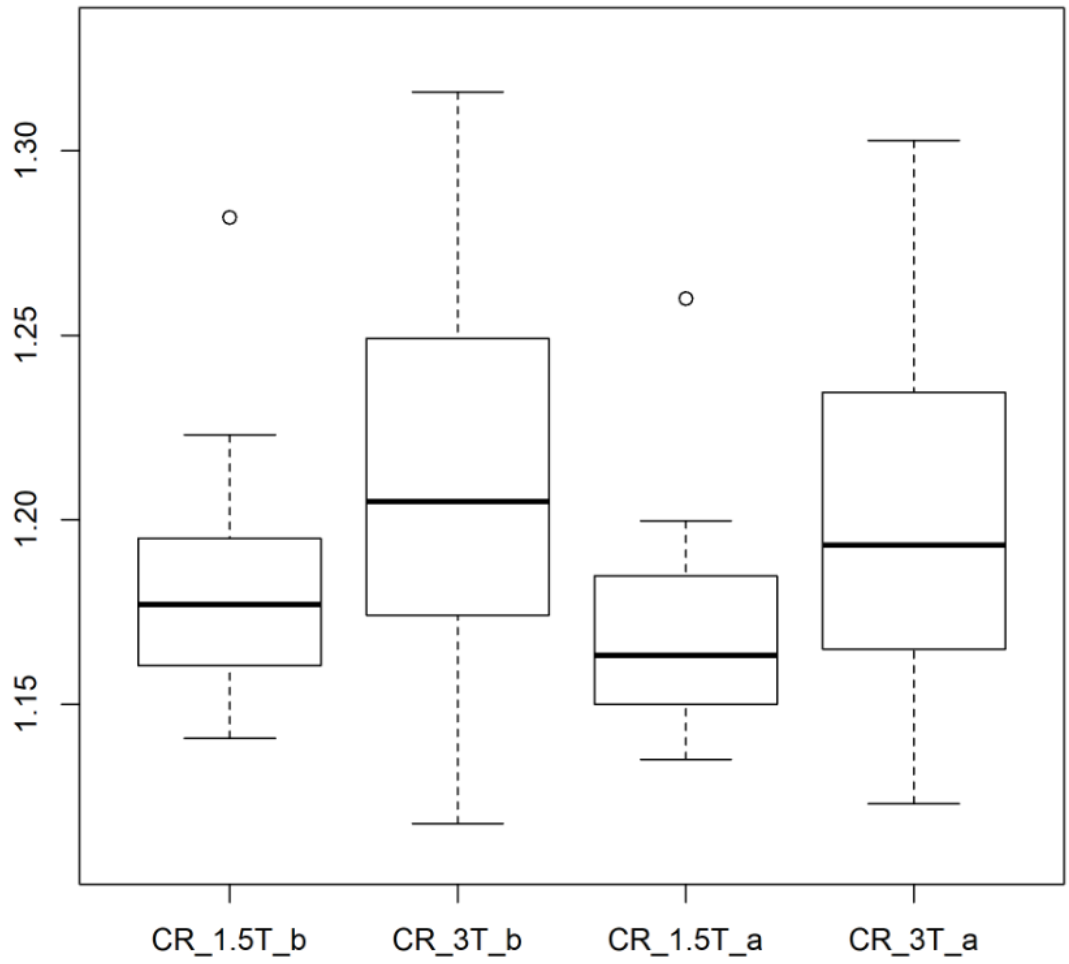

Figure 3.12: Dispersion of contrast ratios (CR) of *Substantia nigra* at 1.5T and 3T, before (left side) and after (right side) the *Gaussian blur* filter application. In both cases, no significant difference was found between field strengths, although the median CR was lower for 1.5T than 3T.

Semi-automatic algorithm			Median (Q1-Q3)	Friedman (p-value)	ICC	CI
Area (mm^2)	1.5T	S1	28.6 (19.5 - 30.8)	0.5308	0.815	0.676 - 0.908
		S2	25.2 (17.9 - 30.6)			
		S3	26.7 (20.4 - 32.1)			
	3T	S1	23.3 (20.8 - 32.0)	0.9893	0.913	0.837 - 0.958
		S2	23.0 (18.5 - 30.8)			
		S3	23.1 (20.0 - 30.3)			
DSC	1.5T	S1	0.72 (0.68 - 0.79)	0.9892	0.817	0.677 - 0.909
		S2	0.71 (0.66 - 0.78)			
		S3	0.73 (0.68 - 0.77)			
	3T	S1	0.76 (0.72 - 0.79)	0.2430	0.777	0.617 - 0.887
		S2	0.77 (0.71 - 0.80)			
		S3	0.78 (0.73 - 0.83)			

Table 3.1: ICC and Friedman test results for repeated SN area estimates obtained with the semi-automatic segmentation algorithm at both field strengths and DSC between the semi-automatic SN regions-of-interest (ROI) and corresponding manual ROI. Q1-Q3 represents the range of the box - from the lower quartile (Q1) to the upper quartile (Q3). ICC: intraclass correlation coefficient, 95% CI: confidence interval, DSC: dice similarity coefficient.

3.3 Discussion

Segmentation of the SN using NM-MRI has been previously applied mainly at 3T to differentiate between PD and controls [40] and to investigate disease progression by comparing between PD groups [69]. Since differences between SN areas may be subtle, it is important to guarantee a good reliability of the segmentation method. This is particularly relevant for application of the methodology at 1.5T, as the CR is lower than at 3T and because the segmentation method had been previously optimized for the SN visualization at 3T [71].

To evaluate the quality of the segmentation at both field strengths, ROI manual delineation was used as the gold standard, despite being time consuming and operator dependent, as it is the only method that ensures a good anatomical correlation. Area and spatial distribution comparison between semi-automatic and corresponding manual segmentation revealed an excellent agreement between methods and hence, an excellent reliability of the semi-automatic algorithm for both field strengths.

An excellent repeatability was obtained for the SN measurements (area and DSC) with high ICC values at both field strengths (Table 3.1), indicating a good level of reliability of the semi-automatic segmentation procedure. Even so, the SN measurements at 1.5T presented a wider confidence interval and a slightly reduced agreement compared to 3T. The most likely explanation is that since region growing segmentation relies on image contrast to delineate the included region, and as 1.5T images have lower CR (Figure 3.12), segmented regions tended to be more variable. Consequently, the algorithm's precision was diminished at 1.5T as expected. Nevertheless, the semi-automatic segmentation algorithm is reproducible at 1.5T.

While studying differences in contrast ratio between field strengths, two possible CR measurements were tested: before and after the application of the *Gaussian blur* filter - first step of the SN segmentation pipeline. The CR measured after the filter application is statistically smaller when compared to the original CR measures, which is expected considering that the said filter blurs the image, thus diminishing the contrast. Nevertheless, despite image filtering altered the measured CR, the percentage difference is much smaller than between images acquired with different field strengths. In addition, when comparing CR differences between field strengths, regardless of image filtering, differences are observed. Therefore, SN CR differences between field strengths can be evaluated after the filter application. In fact, such differences may be responsible for the wider variability of the semi-automatic SN areas at 1.5T.

Another factor that may lead to errors in ROI analyses is related to the anatomical training of the observer, as the measurement method partly depends on the placement of the *seed region* made by the observer. In the future, it would therefore be beneficial to evaluate the interrater reliability associated to these SN ROI measurements.

In this study, the small positive bias observed with the Bland-Altman method between scanners is an indicative that, on average, the segmented areas measured at different magnetic fields were similar, with the 1.5T segmented SN areas appearing to be slightly

larger than at 3T. This increase of the 1.5T segmented SN areas over the 3T measurements can be due to the lower CR present in 1.5T NM-sensitive images, which leads to a reduced precision in the delineation of the SN ROI. Nevertheless, the observed limits of agreement between ROIs taken from images collected with different magnetic fields were wide. A few factors (differences in SNR, CR, head positioning, and potentially motion artifacts) could all have contributed to these variabilities.

A further source of variability, in the study between field strengths, is the difference in spatial resolution of the two sequences as a slightly coarser resolution was used at 1.5T to minimize SNR differences, as explained in section 3.1.2.1. It is common for these types of studies, which investigate differences between similar MRI sequences, to try to maintain as many parameters with the same value, in order to reduce sources of variability [51]. However, in this case, spatial resolution at 1.5T was altered for the referred reason and resolution at 3T (the standard clinical sequence) had to be maintained to not compromise the comparison as a mean for validation. Parallel imaging acceleration was not employed at 1.5T for the same reason, despite resulting in a longer acquisition time. Since the scanner only provided the final averaged images, and as PI was used at 3T, SNR could not be reliably evaluated at 3T [75] and it was therefore not compared between field strengths.

Even though the two scans for each subject were made on the same day, head positioning is likely to have varied between exams. On this note, the DSC of the SN areas was not compared between field strengths, as differences in head positioning could alter the true spatial overlap of said measurements. It would therefore be necessary to evaluate whether head positioning introduced significant variability in the evaluated SN regions. A previous study [70] investigated the repositioning effect between scans and observed no significant differences in SN measurements. However, in that study, only the contrast variations with head positioning were accounted for, since the different images were co-registered to a common reference.

Another important issue in NM-MRI is head motion artefacts, which can be increased due to clinical symptoms, especially in cases of PD, such as tremors and aggravated due to the long duration of these sequences. Averaging images acquired at different positions may result in a final image with diminished quality [51]. Although 3D sequences are associated to higher SNR, they are typically more sensitive to motion. In this study, a 2D sequence was applied, as these typically have shorter acquisition times, consequentially reducing the potential for motion artefacts.

The SN area was measured in a single slice (middle slice), as opposed to evaluating the whole SN volume, to reduce partial volume effects occurring in the outer portions due to the thick slices that had to be used (2.5mm) to ensure sufficient SNR. In addition, 2D segmentation of a single slice is simpler and faster and therefore more easily included in clinic practice.

Additionally, even though the CR was not significantly different between field strengths, CR at 1.5T was lower than at 3T introducing variability in the SN measurements. In this study various sources of variability could have influenced the agreement of the SN

measurements between field strengths. Nevertheless, the tested semi-automatic algorithm revealed to be reliable at 1.5T.

This study has some limitations, namely the small sample size (12 patients), although the number is not very different from other published NM-MRI studies (range 6-11 subjects) [49, 51, 70] and the statistical tests were performed taking the sample size into account.

CHAPTER 4

Adaptation of the 1.5T NM-MRI sequence for DBS patients

In order to evaluate whether Deep Brain Stimulation has any observable effect on the SN area, it is necessary to develop a 1.5T NM-sensitive sequence that is not harmful to PD patients with these systems implanted and is in compliance with all DBS-MRI conditions - as mentioned in Section 2.3.2. Adding to this, the developed sequence must allow a good visualization of the NM-SN area. In this chapter, the 1.5T sequence developed to scan patients with implanted neurostimulators is presented and discussed. To assess its feasibility in depicting the SN area, a comparison of the SN areas measured with a semi-automated method was made between the referred 1.5T DBS sequence and the 1.5T sequence previously validated in Chapter 3. In addition, the results obtained using the 1.5T DBS sequence in a patient after surgical placement of the DBS electrodes are also presented.

4.1 Materials and Methods

4.1.1 Sample Description

This study included a cohort of six individuals (4 males and 2 females), with ages ranging from 31 to 70 years (mean age: 43.5 ± 14.61 years). All subjects presented movement-related disorders, with an undetermined diagnosis. Patients were recruited from the Movement Disorders Unit of Hospital of Santa Maria-Lisbon.

The 1.5T DBS sequence was tested in a 60 years-old male PD patient, also included in the previous study comparing NM-MRI sequences between field strengths - Chapter 3.

All examinations in this study were performed with the understanding and informed consent of each subject.

4.1.2 Imaging Protocol

In order to investigate the effects of DBS in the SN through NM-MR imaging of patients with implanted neurostimulators, the 1.5T NM-MRI sequence previously developed and validated in Chapter 3 had to be adapted to ensure that all DBS-related MRI limitations were accounted for. The necessary adaptations made to the acquisition parameters are discussed in 4.1.2.1.

Once again a comparative study was performed, this time between the two developed 1.5T NM-MRI sequences to investigate potential differences in segmentation reproducibility and image contrast.

The acquisition parameters of the previously validated 1.5T sequence, from here on designated as general sequence, were: TR/TE of 600/10ms; turbo factor of 3; FOV of 220×180 mm^2; matrix size of 440×361 (pixel size of 0.50×0.50 mm^2); slice thickness of 2.5mm with no gap; four averages; no PI and an acquisition time of 9:45 min.

The 1.5T sequence adapted to scan patients with implanted DBS systems, from here on referred to as DBS sequence, had the following acquisition parameters: repetition time/echo time of 750/9.5ms; turbo factor of 3; FOV of 220×189 mm^2; matrix size of 440×375 (pixel size of 0.50×0.50 mm^2); slice thickness of 2.5mm with no gap; four averages; PI with reduction factor of 1.5 and an acquisition time of 8:33 min.

All images were acquired using a T_1–weighted FSE sequence with an 8-channel SENSE head coil. All data were acquired with a 1.5T MRI system (Intera 1.5, Philips Medical Systems, Best, Netherlands). Each subject underwent two scans – one for each 1.5T sequence - in the MRI system, with both acquisitions being performed during the same exam.

The PD patient was examined a single time with the 1.5T DBS sequence 3 months after the implantation of the DBS system. These images were taken 5 months after the initial scans with the 3T and general 1.5T NM-MRI sequences.

The sections were carefully set in the oblique axial plane perpendicular to the floor of the fourth ventricle, starting from the posterior commissure to the inferior border of the pons.

4.1.2.1 Analysis of the acquisition parameters

Patients with implanted neurostimulators can only be safely imaged with 1.5T MRI systems and following certain conditions, as previously described in Section 2.3.2. The general 1.5T sequence, which already fulfills a very important condition for DBS imaging – scanning with a 1.5T MRI system, showed sufficient image contrast to enable SN segmentation. However, the parameter B_{1+RMS} has to be less than or equal to 2.0 μT in order to guarantee a safe examination.

In order to ensure that B_{1+RMS} stayed within safety limits, the repetition time (TR) was increased, from 600ms to 750ms, considering that an increase in TR leads to a reduction in the B_{1+RMS} (1.98 μT). This TR increase can improve SNR as it increases

the magnetization present in each voxel, but it also results in a longer scan acquisition. Considering that the scan duration of the general sequence was already substantially long (9:45 min), this added time increase, which resulted from the alteration of the TR, should be compensated in order to diminish potential image artefacts and discomfort to the patients. Thus, parallel imaging with SENSE was activated once again, like it was in the original 3T sequence, with the same reduction factor of 1.5, enabling a faster acquisition (8:33 min).

The pixel size was maintained the same (0.5x0.5) to ensure the same spatial resolution, hence reducing variability sources between the two tested 1.5T sequences.

4.1.3 Imaging Analysis

All image processing was performed using the OsiriX program (Version Lite) [68].

In order to validate the developed 1.5T NM-MRI sequence optimized for patients with implanted neurostimulators, the segmentation method that allows quantitative measurement of the SN, previously described in Section 3.1.3.1, was applied to the SN on both sides of the brain for every single patient. Considering the left and right regions-of-interest of each image as independent regions, a total of 12 regions-of-interest were analyzed.

In the present study, the semi-automated segmentation method was performed three times for each ROI in order to verify the feasibility of the algorithm. The repeated measures were taken on different days to avoid biasing.

The CR was calculated after the *Gaussian blur* filter application using the method previously described in Section 3.1.3.3. In order to assess CR differences between the 1.5T NM-MRI sequences, ROI measurements were kept in the exact same position between sequences.

For the DBS patient, a single measurement of the SN area was performed with the semi-automatic algorithm for both sides of the brain. The CR was also measured with the method described above.

4.1.4 Statistical Analysis

All statistical analyses were performed with the R software, version 3.3.3. (R Foundation for Statistical Computing, Vienna, Austria), considering a *p-value* lower than 0.05 as significant.

The Friedman test was applied to the three SN estimates of each ROI, in order to evaluate statistical differences within repeats. Additionally, a two-way random ICC evaluating absolute agreement was performed to assess the algorithm's repeatability. The ICC value and its 95% CI were calculated and interpreted according to the criteria set by Landis and Koch [73].

In order to assess the reproducibility of the segmented SN areas between the two tested 1.5T MRI sequences, the Wilcoxon signed rank test was applied to the corresponding paired SN areas, as well as the Bland-Altman method.

The Wilcoxon test was also used to investigate differences in the CR measured with the two 1.5T NM-sensitive sequences.

4.2 Results

No significant differences were observed with the Friedman test for either 1.5T sequences when comparing between the three repeated estimates of the SN area (Table 4.1). Moreover, higher *p-values* were obtained with the general 1.5T sequence (p=0.8139) than with the DBS-optimized sequence (p=0.7408).

The repeatability of the semi-automatic algorithm still needed to be assessed. To that end, the ICC and CI of the repeated SN areas estimated with the semi-automatic algorithm were calculated - Table 4.1. A high ICC was obtained for both 1.5T tested sequences. The SN areas measured with the general sequence presented a slighter higher and narrower CI ($CI_{general}$: 0.743 – 0.964, p<0.001) when compared to the 1.5T sequence optimized to scan patients with implanted DBS systems ($CI_{general}$: 0.611 – 0.941, p<0.001). Nevertheless, both sequences showed a substantial to almost perfect agreement between repeated measures.

The segmented SN areas estimated with the semi-automatic algorithm showed excellent test-retest reliability, justifying the usage from here on of a single sample of the areas corresponding to the ROIs in the analysis.

The Wilcoxon test comparing the area of the same SN regions between sequences revealed a non-significant difference (*p-value*=0.9097) between said estimates. Adding to this, the analysis with Bland-Altman plot of the SN areas showed good agreement between the semi-automatic measures obtained with the different sequences (Figure 4.1) with an approximately null bias. Its limits of agreement ranged from -12.20 mm^2 to 12.20 mm^2, which is narrower than the range obtained from the agreement between field strengths (Figure 3.11).

When comparing the corresponding CRs between the 1.5T NM-MRI sequences, the Wilcoxon test showed no significant difference with a *p-value* of 0.8438. The median CRs of the 1.5T sequences were approximately the same ($CR_{general}$: 1.151; CR_{DBS}: 1.150) - Figure 4.2. Nevertheless, the range of the 1.5T general sequence [1.131 - 1.239] was narrower than the 1.5T DBS sequence [1.094 - 1.267].

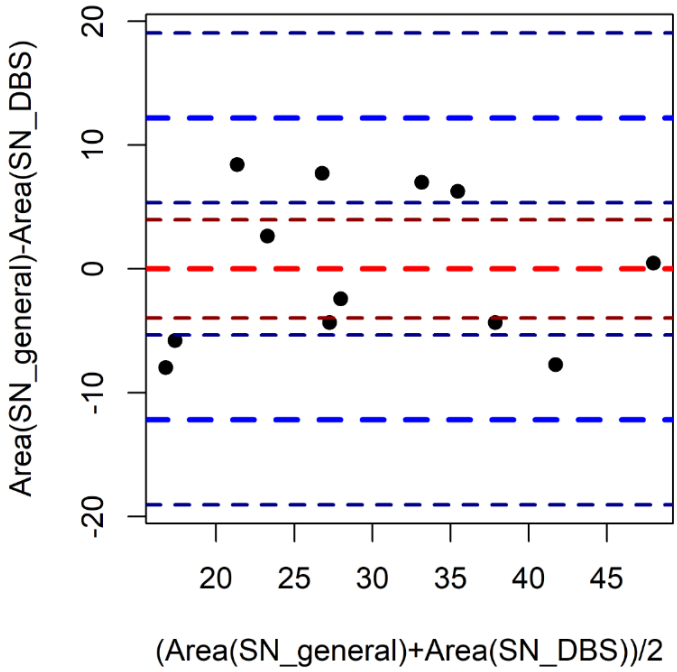

Figure 4.1: Agreement analysis of SN areas between the two different 1.5T sequences – general and optimized for DBS. The plot shows a null bias between the mean differences and an agreement interval ranging from -12.20 mm^2 to 12.20 mm^2, with a 95% confidence interval.

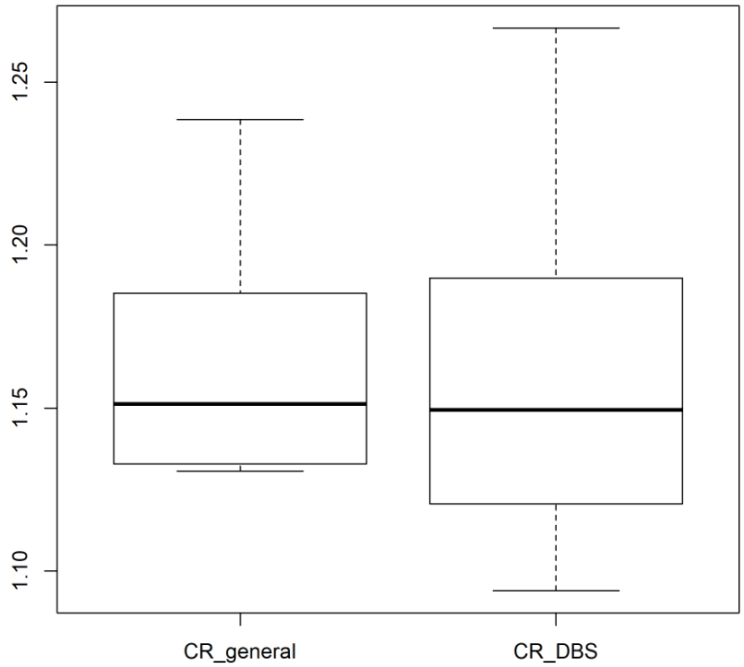

Figure 4.2: Dispersion of the SN CR after the *Gaussian blur* filter application, with the general 1.5T sequence (left) and the DBS 1.5T sequence (right). No significant difference was found between the 1.5T NM-MRI sequences.

Semi-automatic algorithm		**Area (mm^2) Median (Q1-Q3)**	**Friedman (p-value)**	**ICC**	**CI**
general	Sample 1	29.5 (24.1 - 35.5)	0.8139	0.892	0.743 - 0.964
	Sample 2	28.7 (24.8 - 37.3)			
	Sample 3	31.5 (25.1 - 37.1)			
DBS	Sample 1	28.1 (20.5 - 36.8)	0.7408	0.825	0.611 - 0.941
	Sample 2	29.3 (21.3 - 36.2)			
	Sample 3	27.5 (21.3 - 37.6)			

Table 4.1: ICC and Friedman test results of the comparison between the three repeated SN area estimates obtained with the semi-automatic segmentation algorithm, for the general 1.5T NM-MRI sequence developed previously and 1.5T NM-MRI sequence optimized to scan patientes with implanted DBS systems. Q1-Q3 represents the range of the box - from the lower quartile (Q1) to the upper quartile (Q3). ICC: intraclass correlation coefficient, 95% CI: confidence interval.

The obtained images and the SN areas, measured with the semi-automatic algorithm, of the DBS patient are presented in Figure 4.3 and Table 4.2, respectively, jointly with the corresponding results obtained previously with the 3T and general 1.5T NM-MRI sequence. The right SN area measured in this case was substantially reduced when compared with the measurements performed with the other NM-MRI sequences, in agreement with what can be observed with the images. The left SN area is very similar to the corresponding SN area obtained with the 1.5T general sequence and not much smaller in comparison with the 3T sequence. However, despite presenting similar sizes, the spatial distribution of the SN area observed in 4.3a appears to be slightly altered. The CR calculated with the 1.5T DBS sequence was very similar, although slightly smaller (1.114) than the CR obtained at 3T (1.123). The CR measured with the 1.5T general sequence was unexpectedly higher than at 3T (Table 4.2), which must have been a statistical anomaly considering the CR observations in Chapter 3.

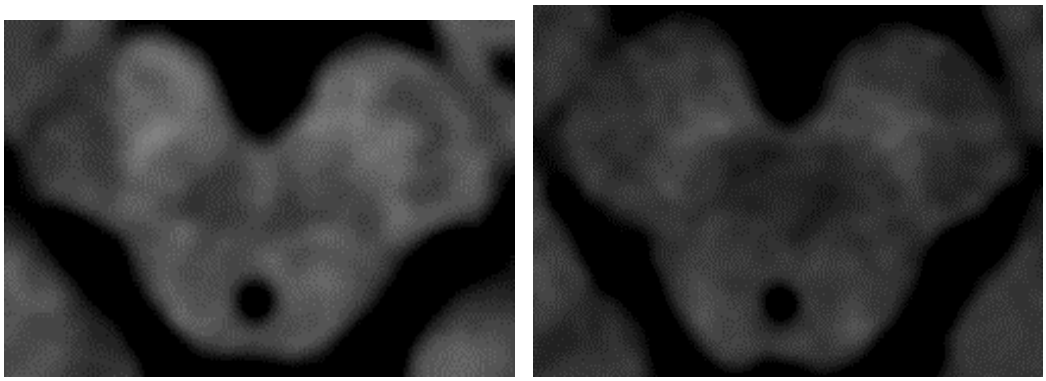

a DBS sequence

b general 1.5T sequence

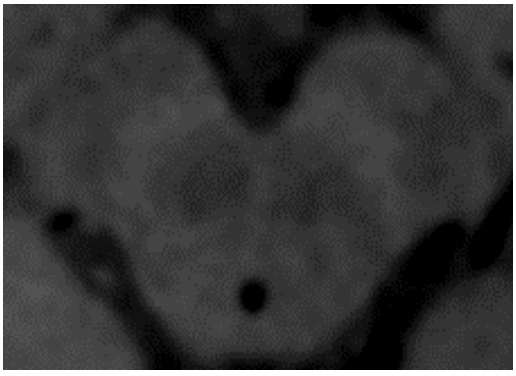

c 3T sequence

Figure 4.3: Axial sections at the level of the midbrain showing the SN area of the same patient, taken with three different NM-MRI sequences - 1.5T DBS sequence (a), 1.5T general sequence (b) and 3T sequence (c). Image (a) was taken after surgical placement of DBS electrodes.

		DBS	general 1.5T	3T
Area (mm^2)	Right side	9.5	26.0	35.0
	Left side	31.2	32.3	40.1
CR		1.114	1.199	1.123

Table 4.2: SN areas of the same patient measured with the semi-automatic algorithm in three different NM-MRI sequences - 3T and general 1.5T sequences in the same day and DBS sequence after the surgical intervention.

4.3 Discussion

When evaluating the reliability of the semi-automated method between the two 1.5T NM-MRI sequences, a simpler comparison than the one made in Chapter 3 was performed measuring only the semi-automated areas. This decision was made due to the smaller sample size of this study (6 subjects) and considering that the semi-automatic SN measures showed good spatial agreement with the manual measures for both field strengths, even though it was more likely to observe SN differences between field strengths.

The test-retest agreement (repeatability) of the semi-automated SN measures using the 1.5T DBS sequence revealed a substantial to almost perfect agreement, as the general 1.5T did. Despite the agreement measured with the ICC was slightly smaller comparing to the general 1.5T sequence, their similar results may indicate that the semi-automatic algorithm is reproducible with the 1.5T DBS sequence. Additionally, the 1.5T general sequence ICC results for the SN areas obtained in Chapter 3 were slightly worse, even with a greater sample size.

The comparison between 1.5T sequences with the Bland-Altman method, showing a null bias, indicates that, on average, the segmented areas have the same size. This was a very positive result, especially considering the small sample size, and even though the obtained range was narrower than the one obtained between field strengths, it was still substantial. A few factors (differences in SNR, CR, and motion artifacts), some already previously discussed in section 3.3, could have contributed to this wide range of agreement between the SN areas.

Considering that no significant difference was observed between the CRs of the 1.5T sequences and that their median values were very similar, it is likely that CR was not the main factor to influence the variability of the SN areas. Still, the slightly wider range of CR obtained with the DBS sequence may contribute, in part, to the SN area variability. As it was previously discussed, the image contrast influences the delineation of the SN area with the semi-automatic algorithm.

Once again, SNR evaluation could not be performed between the 1.5T sequences because PI was employed in one of the sequences. The 1.5T DBS sequence had to compensate for the time increase that resulted from the necessary changes for examination.

In a previous study at 3T [51], it was demonstrated that GE sequences with MT pulses can generate NM-sensitive images with improved contrast in comparison with FSE

sequences with no additional MT pulse, since the latter sequence relies only on incidental MT effects. Nevertheless, in this study, in order to carry out the clinic practice's needs, a FSE sequence was chosen to investigate feasibility of the semi-automatic segmentation algorithm in 1.5T sequences befitting the necessary conditions to scan DBS patients. The same group also investigated the specific absorption rate (SAR) for the two types of NM-MRI sequences and observed a significant decrease in GE sequences [51]. Further studies should compare the performance of these two types of sequences at 1.5T, considering not only the SAR but also the B_{1+RMS} which has been established as a more accurate measure of potential heating, since it is not patient dependent and it does not vary according to the model considered by each MRI manufacturer [39]. Future work should also compare the performance of GE and FSE 1.5T NM-MRI sequences as biomarkers for early detection of Parkinson's disease and to differentiate between disease stages.

Considering a preliminary result of the 1.5T DBS NM-MRI sequence performed on a patient with implanted neurostimulators, the SN area visualization does not appear to be accurate. The right SN area was too small in comparison with the measurements performed with the other NM-MRI sequences. It is difficult to assess whether this reduction in the area is due to lower accuracy in the delineation of the SN associated to lower CR associated to the sequence itself, the presence of the DBS electrodes or even other factors. The study comparing the two 1.5T sequences does not appear to be consistent with this patient. There was only one case in which the 1.5T DBS sequence provided poorer SN visualization, nevertheless the study's sample size was very small. In both comparisons between sequences (Chapters 3 and 4), even though the SN areas revealed to have the same size on average, the wide variability observed prevents reliable conclusions to be inferred from a single sample. In order to assess potential effects of DBS therapeutic in the NM-SN, the 1.5T DBS sequence should be tested with a big sample size.

A previous study [47] compared incidental MT effects in FSE sequences at 3T and 1.5T and revealed that incidental MT effects are reduced at 1.5T. This reduction is likely to be the reason for the observed reduction in CR and hence wider variability of the SN areas. In addition, the applied TR increase in the DBS sequence can possibly be affecting the T1-shortening effects, which would also contribute to a worse delineation of the SN. Future work should test if different TRs influence the SN delineation and how other parameters, such as reducing the Turbo factor, could be managed in order to optimize the 1.5T DBS sequence. Another possible source for the reduced contrast observed with the DBS patient could be the presence of the implanted electrodes (Figure 4.4). The electrodes could potentially alter the homogeneity of the magnetic field and hence influence the resulting image contrast.

Finally, another important factor to be considered is the variability related to head positioning and slice orientation. This examination was performed on a different day, unlike the images taken for the other two studies, which were either at least on the same day or during the same examination. As previously discussed, head positioning may not have much influence on the image contrast as demonstrated in [70]. However, the

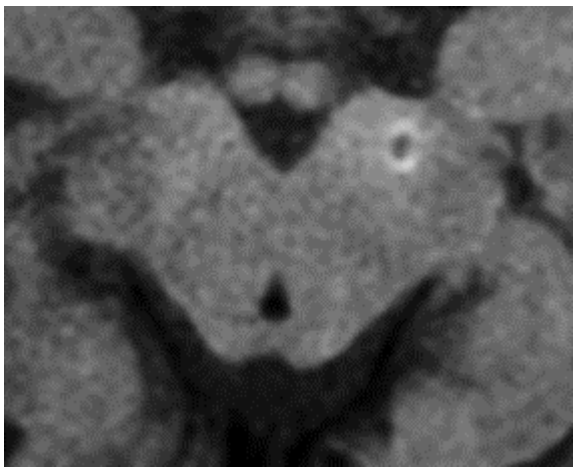

Figure 4.4: Axial section at the level of the upper midbrain of the DBS patient. The left DBS electrode is still visible in this slice, which is adjacent to the slice chosen for SN measurements. These slices are only distanced 2.5mm - the chosen slice thickness.

repositioning effect is likely to be influencing our segmentation, since it is performed in a single slice. In the future it would be important to carry out a study that evaluates the area variability associated with alterations in slice angulation and invest in a 3D sequence and segmentation method in order to reduce the referred effect.

CHAPTER 5

Imaging Study of therapeutic effects on PD patients

PD symptoms are very incapacitating but fortunately, through therapeutics, such as medication or surgery, such symptoms can be eased. Recently many studies have been assessing the application of NM-MRI as a diagnostic biomarker for PD and also as a means to further investigate the disease. In order to investigate potential effects of therapeutics in the SN progression, in this chapter are presented the results of a study on the medication effects in the SN using NM-MRI. Using a 3T NM-MRI sequence, a comparison was made between SN areas of a PD *de novo* group taken before and after two months of initiating the medication.

5.1 Review on the dopamine metabolism

Parkinson's disease symptoms can be significantly modified with medication, mainly with L-dopa or dopamine agonists [76]. Even though both drugs contribute to an alleviation of symptoms, its consequences on the dopamine metabolism and in turn on the course of PD, are still unclear. Investigating the influence of the medication on the SN NM signal could contribute to a better understanding of the effects of this therapeutical intervention in PD.

As previously described, in PD there is a loss of pigmented dopaminergic neurons of the SN, which produce a chemical - Dopamine (DA) – relevant in the control of motor activity. DA can be transformed trough oxidation into an intermediate product - DA-quinone, usually chelating metals, especially iron. These DA derivatives are then transformed into aminochrome, which is a precursor for the neuronal pigment neuromelanin. The role of iron in the NM production is essential, seeing that it protects the cell from oxidative stress [77] (Figure 5.1).

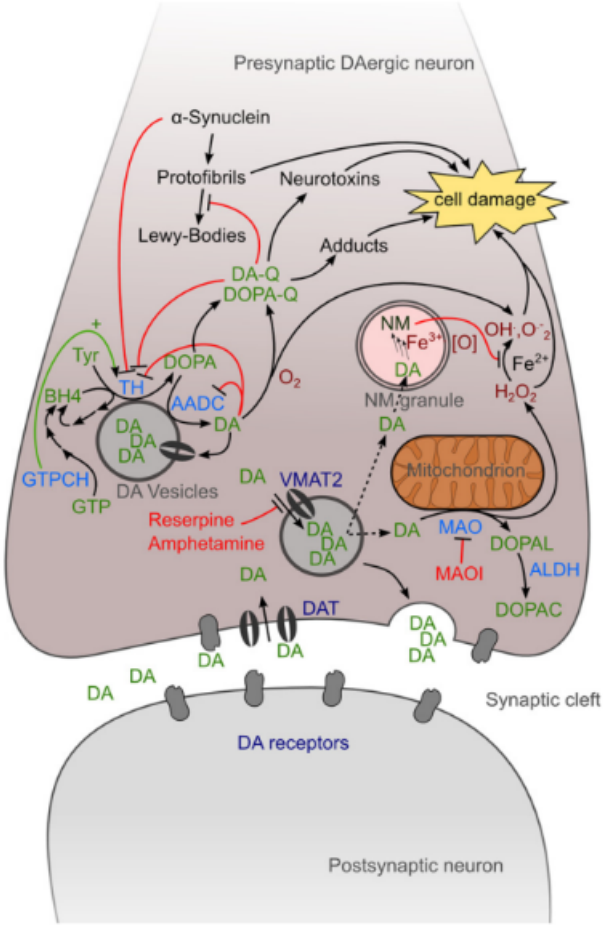

Figure 5.1: Dopamine metabolism on a DAergic neuron. NM is built out of DA oxidation products and chelates iron, staying confined in cytoplasmatic vesicles. When DA is released in the presynaptic DAergic neuron, auto-oxidation or MAO of DA can contribute to cell damage. There are several other DA-related mechanisms that may lead to neuronal death. Adapted from [77].

L-dopa is a precursor for endogenous DA production in the presynaptic dopaminergic neurons of the striatum. During an initial stage of the L-dopa administration, there is a regenerator and protective effect, alleviating the symptoms [78]. However, over time, "the capacity of the nigrostriatal DA system to store and release dopamine is lost" [76], leading to motor complications.

It is believed that L-dopa contributes to oxidative stress, thereby accelerating the progression of PD. If there were a dysfunction in storing DA, the excessive released dopamine could lead to free radicals formation through MonoAmine Oxidation (MAO) and consequently, oxidative stress [78] (Figure 5.1). Therefore, considering the long-term consequences of L-dopa, dopamine agonists have been increasingly used as an alternative in alleviating the clinical features of PD [76].

Dopamine agonists can influence postsynaptic DA receptors on the striatum and presynaptic receptors in the SN. Noting that dopamine agonists (exogenous DA) do not depend

on the capacities of the nigrostriatal neurons, this medication may prevent free radical formation as a result of endogenous DA metabolism [76]. In addition, a study demonstrated that SN neurons show comparatively low MAO presence when compared with other neurons [79].

5.2 Materials and Methods

5.2.1 Sample Description

The present study included a cohort of six individuals (3 males and 3 females), with ages ranging from 46 to 82 years (mean age: 64.2 ± 14.3 years). All subjects were diagnosed with Parkinson's disease by a movement disorders specialist according to the PD UK Brain Bank criteria [66] and were rated using the UPDRS. Patients were recruited from the Movement Disorders Unit of Hospital of Santa Maria-Lisbon.

The PD patients, denominated as PD *de novo* in this study, were included at the time of their first diagnosis if they were not taking any anti-Parkinson medication and were considered to be at an initial stage of the disease. It was considered early stage of the disease if the patients had been diagnosed within 6 months of the first symptoms.

The examinations were performed with the understanding and informed consent of each subject. These images had already been used in a previous work [80].

5.2.2 Imaging Protocol

In order to assess potential effects of pharmacological medication on the signal of NM-SN in patients first receiving medication, the PD group underwent two MRI acquisitions over time. The first acquisition was performed at the time of the diagnosis, before the patients took any anti-Parkinson medication, and the second scan was performed two months after initiating medication. All patients were treated with the dopamine agonist - Ropinirole -, initiating with a dose of 2mg/d, 4mg/d and 6mg/d, respectively, in the first 3 weeks and continuing the treatment with a stable dose of 6mg/day.

All images were collected using a 3T MRI (Achieva 3.0, Philips Medical Systems, Best, Netherlands) system with a 32-channel SENSE head coil. The used MRI sequence was a T_1–weighted FSE; the same as the 3T sequence described in 3.1.2. To obtain the desired images of the *substantia nigra*, the sections were carefully set in the oblique axial plane perpendicular to the floor of the fourth ventricle, ensuring coverage from the posterior commissure to the inferior border of the pons.

5.2.3 Imaging Analysis

The segmentation algorithm used in this study for the measurements of the SN areas was the same as the previously described in Section 3.1.3.1.

The same procedure was used for all images, which included firstly the application of the *Gaussian blur* filter and then the segmentation using the *Confidence* algorithm, followed by the application of *Brush Closing* to remove any holes in the delineated ROI. A single SN area estimate was calculated for every ROI, using the semi-automatic segmentation algorithm. The estimates for the different scans – at the time of diagnosis and two months after initiating medication – were performed on different days. The measured areas of the SN were recorded for both sides of the brain.

5.2.4 Statistical Analysis

All statistical analyses were performed with the R software, version 3.3.3. (R Foundation for Statistical Computing, Vienna, Austria), considering a *p-value* lower than 0.05 as significant.

In order to assess potential effects of anti-Parkinson medication in the SN area, the Wilcoxon signed rank test was applied to the corresponding paired SN areas – estimated before and after medication.

The Wilcoxon test was also used to investigate differences in the UPDRS scores (part III, corresponding to motor examination, and total) rated before and after the initiation of medication. However, only five subjects were accounted for this comparison, considering that one of the subjects dropped out of the study and his UPDRS score after two months of initiating medication was not evaluated.

5.3 Results

No significant differences (*p-value*=0.1514) were detected when comparing the SN areas determined at the time of diagnosis and after 2 months of initiating medication, using the Wilcoxon pair-wised comparison. However, the dispersion of the SN areas measured before and after medication may suggest a tendency for the median SN area to increase after medication (Figure 5.2).

The Wilcoxon comparison applied to the UPDRS scores (mean score ± standard deviation) - part III and total - evaluated before ($UPDRS_{III}$: 38±15; $UPDRS_{Total}$: 58±31) and after medication ($UPDRS_{III}$: 40±12; $UPDRS_{Total}$: 62±27) showed no significant differences for either $UPDRS_{III}$ (*p-value*=0.625) and $UPDRS_{Total}$ (*p-value*=0.5879).

5.4 Discussion

Segmentation of the SN using T1-weighted FSE NM-sensitive MRI as an accurate diagnostic tool for discrimination of Parkinson's disease patients from healthy subjects [40] has been increasingly applied. Even more, investigating potential differences in the SN hyper-intense area can contribute to a better understanding of the underlying mechanisms in PD.

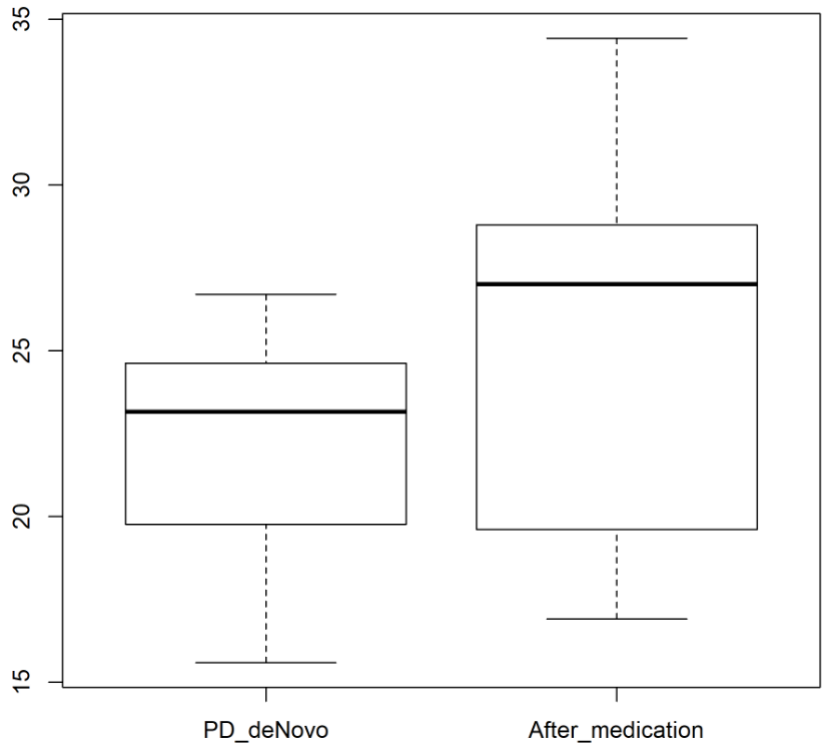

Figure 5.2: Box and whisker plot of the *Substantia nigra* areas estimated from the NM-MR images taken before and after medication. No significant differences were found, although the median SN area was increased after 2 months of medication (27.0 mm^2) compared to at the time of diagnosis (23.2 mm^2).

Recently, a study by Hatano et al. [81] reported a significant reduction in the measured SN area in PD patients displaying motor complications induced by L-dopa medication. However, PD patients with motor complications also had longer disease durations (10±3 years versus 5±3; mean ± standard deviation). In latter stages the significant reduction of neuromelanin can possibly no longer be compensated by the administered dopamine and so the signal is reduced. Therefore, this study intended to assess potential changes of the NM MR signal in drug naïve patients at an initial stage of the disease.

The dopamine agonist Ropinirole was chosen as the administered pharmacological medication, considering that DA agonists, unlike L-dopa, are believed to have a more protective and healing effect, preventing further motor complications over time. Thus, this study investigated potential effects on the signal of NM in the SN in patients first receiving DA agonists.

Although the Wilcoxon test showed no significant difference between the SN areas estimated before and after medication, the median SN area tended to be increased after medication (Figure 5.2). This finding may be related to the increase of neuromelanin, related to the dopamine therapy.

Ropinirole has a selective activity at D2 and D3 dopamine receptors, which are localized postsynaptically on striatal neurons and presynaptically in the SN [82]. Considering that

NM is derived from DA oxidation products in the presynaptic dopaminergic neurons of the SN and that the selected dopamine agonist leads to activation of these dopamine receptors, the administration of this medication could explain the increase on the NM-SN hyper-intense MR signal.

In spite of the tendency for the SN area to increase, both UPDRS values (motor-related and total) did not show a significant change. In fact, the overall median UPDRS scores even revealed a slight increase. However, it is common for the UPDRS scores to increase even when the patients are taking ant-Parkinson medication and, specifically at an earlier stage of pharmacological treatment, their response to the treatment is usually slow and not always positive. Therefore, studying the influence of medication on the SN MR signal only after two months of initiating it, may have been a period too small for significant differences to be observed and, in the future, a positive response by the patients should be guaranteed.

Furthermore, this study was performed with a very small sample size (6 subjects) and no significant differences on the measured SN areas caused by medication were observed, only a slight tendency. Therefore, further studies, with larger samples, are needed to corroborate these findings.

CHAPTER 6

Conclusions and Future Work

6.1 Conclusions

The main goal of the present work was to obtain a 1.5T NM-sensitive MRI sequence that enables an accurate measurement of the NM-SN area of patients with implanted Deep Brain Stimulation systems. To achieve that, firstly, being aware of how MRI parameters interact with each other and influence the resulting image, the currently used 3T NM-MRI sequence was adapted so it could be used at a 1.5T MRI system, providing images whose quality sufficed for an accurate SN segmentation. On a second phase, the 1.5T NM-MRI sequence was adapted to guarantee the necessary conditions to scan patients with implanted neurostimulators, presenting a B_{1+RMS} of 1.98 μT. In addition, in order to validate the developed NM-MRI sequences, a semi-automatic algorithm optimized for SN segmentation was evaluated resorting to a test-retest agreement analysis. The repeatability of the algorithm revealed to have a substantial to almost perfect agreement, for all tested sequences. The Bland-Altman method showed a small bias between field strengths, even though the CR tended to be lower at 1.5T, suggesting a good agreement, on average, between the SN areas. The DBS sequence presented very similar results, revealing a null bias between the 1.5T SN measures. Despite the good agreement, on average, observed for both comparisons, wide limits of agreement, which could have been influenced by a few factors (differences in SNR, CR, head positioning and motion artefacts), were obtained. In conclusion, this study not only validated the reliability of the semi-automatic segmentation algorithm, but it also presented a feasible 1.5T NM-MRI sequence that allows correct SN delineation. This sequence could potentially enable the assessment of disease progression on these particular cases and lead to a further understanding on PD and on how DBS alters the course of the disease. Furthermore, the 1.5T NM-MRI sequence could be used as an alternative tool for PD assessment when examinations with the 3T MRI scanner is

not a possibility.

Ideally, the 1.5T NM-MRI sequence adapted to scan patients with implanted DBS systems, which enables the measurement of the SN, would have been used to investigate potential effects of this therapeutic in the signal of the NM in the SN of said PD patients. However, the reduced access of the clinic to PD patients scheduled for surgical intervention during the period of this work as well as medical and technical complications regarding those patients prevented the execution of this specific study. Still, the 1.5T DBS sequence was used to scan a single patient after surgical placement of the neurostimulators. The reduced contrast of the image led to a discussion on the factors which could be causing that and prevented to formulate hypothesis on the potential effects of DBS therapeutic in the NM-SN. Future work should be carried out to improve the CR of the 1.5T sequence so that studying the effects of DBS on the NM-SN can become feasible in the future.

Instead, the study performed with PD *de novo* subjects was carried out as an alternative for investigating potential effects of PD therapeutics, specifically pharmacological medication, on the NM-SN signal obtained from neuromelanin-sensitive MRI sequences. In this study, although no significant differences were observed, NM-MR imaging revealed a tendency for the SN area to increase in PD *de Novo* patients after a period of two months of anti-Parkinson medication. This finding may suggest a change in MR signal of the NM related to the increase of dopamine, associated with the administered DA agonists. Nevertheless, these results need to be duplicated in further studies with larger sample sizes. All in all, therapeutic effects in the NM-SN of PD patients opens a path to better understand pharmacological and clinical effects as well as provide a method for treatment evaluation.

At the moment, two articles are being prepared for publishing. One article focus on the feasibility of SN measurements using a 1.5T NM-MRI sequence, adapted in this work, as a method for evaluating DBS effects in the SN of PD patients. The other publication is a short letter which presents the results about the NM-SN alteration under the influence of medication in PD patients.

6.2 Suggestions for Future Work

Along this work, SN area comparisons between sequences were performed. Despite the obtained good agreement, the range of agreement was wide and such could have originated from various sources. Some were studied in this work and others discussed based on previous performed studies. It was not possible to investigate SNR differences between the sequences because only the final averaged images were available with the scanner and in both comparisons, PI was only employed in of the sequences. Nevertheless, this subject should be investigated, if possible between the 3T NM-MRI sequence and the 1.5T DBS sequence.

Regarding the possibility of using the 1.5T NM-MRI sequence as a diagnostic tool for PD, it is of extreme necessity to carry out a case-control study that investigates the

performance of the sequence in detecting differences in the SN for early detection of PD and to differentiate between disease stages. Also, if possible it would be important to perform this study with a bigger sample size.

With respect to the analysis of potential PD therapeutic effects in the SN, which revealed a very interesting result with a tendency for the SN area to be increased as a result of pharmacological medication, it is important to reproduce these results, in the future, with a bigger sample size. In addition, it would be interesting to investigate the iron relation to the neuromelanin formation, as a result of the dopamine oxidation products, and its effect in NM-MRI.

Bibliography

[1] M. A. Brown and R. C. Semelka. *MRI: basic principles and applications*. 3rd ed. Hoboken, New Jersey: John Wiley & Sons, 2003.

[2] Elster LLC. *Questions and Answers in MRI: Spin Echo Variations*. Accessed: 2017-03-24. 2017. URL: http://www.mriquestions.com/se-vs-multi-se-vs-fse.html.

[3] Elster LLC. *Questions and Answers in MRI: Fast spin-echo*. Accessed: 2017-08-27. 2017. URL: http://mri-q.com/what-is-fsetse.html.

[4] Elster LLC. *Questions and Answers in MRI: GRE vs SE*. Accessed: 2017-03-24. 2017. URL: http://www.mriquestions.com/gre-vs-se.html.

[5] Elster LLC. *Questions and Answers in MRI: Image Contrast*. Accessed: 2017-09-15. 2017. URL: http://mriquestions.com/image-contrast-trte.html.

[6] G. Ayano. "Parkinson's Disease: A Concise Overview of Etiology, Epidemiology, Diagnosis, Comorbidity and Management." In: *Journal of Neurological Disorders* 4.6 (2016), pp. 1–6.

[7] S. von Campenhausen, B. Bornschein, R. Wick, K. Bötzel, C. Sampaio, W. Poewe, W. Oertel, U. Siebert, K. Berger, and R. Dodel. "Prevalence and incidence of Parkinson's disease in Europe." In: *European Neuropsychopharmacology*. Vol. 15. 4. Elsevier, 2005, pp. 473–490.

[8] C. F. M. Souza, H. C. P. Almeida, J. Sousa, P. Costa, Y. S. S. Silveira, and J. C. L. Bezerra. "A doença de Parkinson e o processo de envelhecimento motor: uma revisão de literatura." In: *Rev Neurocienc* 19.4 (2011), pp. 718–723.

[9] S.-Y. Chen and S.-T. Tsai. "The epidemiology of Parkinson's disease." In: *Tzu Chi Medical Journal*. Vol. 22. 2. Elsevier, 2010, pp. 73–81.

[10] G. E. Alexander. "Biology of Parkinson's disease: pathogenesis and pathophysiology of a multisystem neurodegenerative disorder." In: *Dialogues in Clinical Neuroscience*. Vol. 6. 3. Les Laboratoires Servier, 2004, pp. 259–280.

[11] Mayfield Clinic. *Parkinson's Disease*. Accessed: 2017-02-02. 2016. URL: http://www.mayfieldclinic.com/PE-PD.htm.

[12] R. F. Pfeiffer, Z. K. Wszolek, and M. Ebadi. *Parkinson's Disease*. 2nd ed. New York: CRC Press, 2013.

[13] *Brainstem III: The Midbrain (Organization of the Central Nervous System) Part 1.* Accessed: 2017-09-19. URL: http://what-when-how.com/neuroscience/brainstem-iii-the-midbrain-organization-of-the-central-nervous-system-part-1/.

[14] F. Blandini, G. Nappi, C. Tassorelli, and E. Martignoni. "Functional changes of the basal ganglia circuitry in Parkinson's disease." In: *Progress in Neurobiology.* Vol. 62. 1. Elsevier, 2000, pp. 63–88.

[15] National Parkinson Foundation. *What Is Parkinsons?* Accessed: 2017-02-03. 2017. URL: http://www.parkinson.org/understanding-parkinsons/what-is-parkinsons.

[16] L. C. Triarhou. "Dopamine and Parkinson's Disease." In: *Madame Curie Bioscience Database.* Landes Bioscience, 2013.

[17] C. G. Goetz, B. C. Tilley, S. R. Shaftman, G. T. Stebbins, S. Fahn, P. Martinez-Martin, W. Poewe, C. Sampaio, M. B. Stern, R. Dodel, et al. "Movement Disorder Society-sponsored revision of the Unified Parkinson's Disease Rating Scale (MDS-UPDRS): Scale presentation and clinimetric testing results." In: *Movement Disorders.* Vol. 23. 15. John Wiley & Sons, Inc, 2008, pp. 2129–2170.

[18] R. Katzenschlager and A. J. Lees. "Treatment of Parkinson's disease: levodopa as the first choice." In: *Journal of Neurology.* Vol. 249. Springer, 2002, pp. II19–II24.

[19] L. Zecca, R. Fariello, P. Riederer, D. Sulzer, A. Gatti, and D. Tampellini. "The absolute concentration of nigral neuromelanin, assayed by a new sensitive method, increases throughout the life and is dramatically decreased in Parkinson's disease." In: *FEBS Letters.* Vol. 510. 3. John Wiley & Sons, Inc, 2002, pp. 216–220.

[20] F. A. Zucca, E. Basso, F. A. Cupaioli, E. Ferrari, D. Sulzer, L. Casella, and L. Zecca. "Neuromelanin of the human substantia nigra: an update." In: *Neurotoxicity Research.* Vol. 25. 1. Springer, 2014, pp. 13–23.

[21] Neuroloss. *Parkinson's disease.* Accessed: 2017-08-17. URL: https://neuroloss.wordpress.com/parkinsons-disease/.

[22] D. Dexter, F. Wells, A. Lee, F Agid, Y Agid, P Jenner, and C. Marsden. "Increased nigral iron content and alterations in other metal ions occurring in brain in Parkinson's disease." In: *Journal of Neurochemistry.* Vol. 52. 6. John Wiley & Sons, Inc, 1989, pp. 1830–1836.

[23] L. Zecca, A. Stroppolo, A. Gatti, D. Tampellini, M. Toscani, M. Gallorini, G. Giaveri, P. Arosio, P. Santambrogio, R. G. Fariello, et al. "The role of iron and copper molecules in the neuronal vulnerability of locus coeruleus and substantia nigra during aging." In: *Proceedings of the National Academy of Sciences of the United States of America* 101.26 (2004), pp. 9843–9848.

[24] P. Limousin, P. Krack, P. Pollak, A. Benazzouz, C. Ardouin, D. Hoffmann, and A.-L. Benabid. "Electrical stimulation of the subthalamic nucleus in advanced Parkinson's disease." In: *New England Journal of Medicine* 339.16 (1998), pp. 1105–1111.

[25] A. O. Ceballos-Baumann. "Functional imaging in Parkinson's disease: activation studies with PET, fMRI and SPECT." In: *Journal of Neurology.* Vol. 250. 1. Springer, 2003, pp. I15–23.

[26] Medtronic. *MRI guidelines for Medtronic deep brain stimulation systems.* 2015.

[27] D. B. Lester, T. D. Rogers, and C. D. Blaha. "Neuronal pathways involved in deep brain stimulation of the subthalamic nucleus for treatment of Parkinson's disease." In: *Conference proceedings : 31st Annual International Conference of the IEEE Engineering in Medicine and Biology Society.* 2009, pp. 3302–3305.

[28] J. Kahan, A. Papadaki, M. White, L. Mancini, T. Yousry, L. Zrinzo, P. Limousin, M. Hariz, T. Foltynie, and J. Thornton. "The safety of using body-transmit MRI in patients with implanted deep brain stimulation devices." In: *PLOS ONE* 10.6 (2015), pp. 1–20.

[29] S. A. Mohsin, N. M. Sheikh, and U. Saeed. "MRI induced heating of deep brain stimulation leads: Effect of the air-tissue interface." In: *Progress In Electromagnetics Research* 83 (2008), pp. 81–91.

[30] M. F. Dempsey, B. Condon, and D. M. Hadley. "Investigation of the factors responsible for burns during MRI." In: *Journal of Magnetic Resonance Imaging.* Vol. 13. 4. John Wiley & Sons, Inc, 2001, pp. 627–631.

[31] J. M. Henderson, J. Tkach, M. Phillips, K. Baker, F. G. Shellock, and A. R. Rezai. "Permanent neurological deficit related to magnetic resonance imaging in a patient with implanted deep brain stimulation electrodes for Parkinson's disease: case report." In: *Neurosurgery* 57.5 (2005).

[32] J. Spiegel, G. Fuss, M. Backens, W. Reith, T. Magnus, G. Becker, J.-R. Moringlane, and U. Dillmann. "Transient dystonia following magnetic resonance imaging in a patient with deep brain stimulation electrodes for the treatment of Parkinson disease: Case report." In: *Journal of Neurosurgery* 99.4 (2003), pp. 772–774.

[33] D. Dormont, D Seidenwurm, D. Galanaud, P Cornu, J Yelnik, and E Bardinet. "Neuroimaging and deep brain stimulation." In: *American Journal of Neuroradiology* 31.1 (2010), pp. 15–23.

[34] A. R. Rezai, A. M. Lozano, A. P. Crawley, M. L. Joy, K. D. Davis, C. L. Kwan, J. O. Dostrovsky, R. R. Tasker, and D. J. Mikulis. "Thalamic stimulation and functional magnetic resonance imaging: localization of cortical and subcortical activation with implanted electrodes: technical note." In: *Journal of Neurosurgery* 90.3 (1999), pp. 583–590.

[35] P. S. Larson, R. M. Richardson, P. A. Starr, and A. J. Martin. "Magnetic resonance imaging of implanted deep brain stimulators: experience in a large series." In: *Stereotactic and Functional Neurosurgery* 86.2 (2008), pp. 92–100.

[36] R. Jason Stafford. *Physics of MRI Safety*. PowerPoint slides. Accessed: 2017-09-15. 2011. URL: http://www.aapm.org/meetings/amos2/pdf/59-17207-59975-979.pdf.

[37] William Faulkner, B.S., R.T. *New MRI Safety Labels and Devices. B1+rms as a Condition of Use*. Accessed: 2017-05-02. 2016. URL: http://www.ismrm.org/smrt/E-Signals/2016FEBRUARY/eSig_5_1_hot_2.htm.

[38] Medtronic. *3T Labeling* B_{1+RMS}. 2016.

[39] T. O. Woods. "Standards for medical devices in MRI: present and future." In: *Journal of Magnetic Resonance Imaging*. Vol. 26. 5. John Wiley & Sons, Inc, 2007, pp. 1186–1189.

[40] M. Sasaki, E. Shibata, K. Tohyama, J. Takahashi, K. Otsuka, K. Tsuchiya, S. Takahashi, S. Ehara, Y. Terayama, and A. Sakai. "Neuromelanin magnetic resonance imaging of locus ceruleus and substantia nigra in Parkinson's disease." In: *Neuroreport* 17.11 (2006), pp. 1215–1218.

[41] S. Kitao, E. Matsusue, S. Fujii, F. Miyoshi, T. Kaminou, S. Kato, H. Ito, and T. Ogawa. "Correlation between pathology and neuromelanin MR imaging in Parkinson's disease and dementia with Lewy bodies." In: *Neuroradiology* 55.8 (2013), pp. 947–953.

[42] M. Sasaki, E. Shibata, K. Kudo, and K. Tohyama. "Neuromelanin-sensitive MRI." In: *Clinical Neuroradiology* 18.3 (2008), pp. 147–153.

[43] S. Reimão and J. J. Ferreira. "Neuromelanin MR imaging in Parkinson's disease." In: *The CNS Journal*. Vol. 2. 1. Oruen Ltd, 2016.

[44] H. Oikawa, M. Sasaki, Y. Tamakawa, S. Ehara, and K. Tohyama. "The substantia nigra in Parkinson disease: proton density-weighted spin-echo and fast short inversion time inversion-recovery MR findings." In: *American Journal of Neuroradiology* 23.10 (2002), pp. 1747–1756.

[45] C. Ohtsuka, M. Sasaki, K. Konno, M. Koide, K. Kato, J. Takahashi, S. Takahashi, K. Kudo, F. Yamashita, and Y. Terayama. "Changes in substantia nigra and locus coeruleus in patients with early-stage Parkinson's disease using neuromelanin-sensitive MR imaging." In: vol. 541. Elsevier Ireland Ltd, 2013, pp. 93–98.

[46] J. P. Wansapura, S. K. Holland, R. S. Dunn, and W. S. Ball. "NMR relaxation times in the human brain at 3.0 tesla." In: *Journal of Magnetic Resonance Imaging*. Vol. 9. 4. John Wiley & Sons, Inc, 1999, pp. 531–538.

[47] Y. Chang, S. J. Bae, Y. J. Lee, M. J. Hwang, S. H. Lee, J. Lee, S. K. Lee, and S. Woo. "Incidental magnetization transfer effects in multislice brain MRI at 3.0 T." In: *Journal of Magnetic Resonance Imaging*. Vol. 25. 4. John Wiley & Sons, Inc, 2007, pp. 862–865.

[48] D. W. McRobbie, E. A. Moore, M. J. Graves, and M. R. Prince. *MRI: from picture to proton*. 2nd ed. New York: Cambridge University Press, 2003, pp. 0–393.

[49] T. Nakane, T. Nihashi, H. Kawai, and S. Naganawa. "Visualization of neuromelanin in the Substantia nigra and locus ceruleus at 1.5 T using a 3D-gradient echo sequence with magnetization transfer contrast." In: *Magnetic Resonance in Medical Sciences* 7.4 (2008), pp. 205–210.

[50] S. Naganawa, T. Koshikawa, K. Sato, T. Katagiri, T. Mimura, T. Ishigaki, and I. Aoki. "Pseudostenosis of the internal carotid artery in 3D time-of-flight MR angiography: effects of a magnetization transfer contrast pulse and metallic material." In: *European Radiology*. Vol. 13. 10. Springer, 2003, pp. 2298–2303.

[51] X. Chen, D. E. Huddleston, J. Langley, S. Ahn, C. J. Barnum, S. A. Factor, A. I. Levey, and X. Hu. "Simultaneous imaging of locus coeruleus and substantia nigra with a quantitative neuromelanin MRI approach." In: *Magnetic Resonance Imaging*. Vol. 32. 10. Elsevier, 2014, pp. 1301–1306.

[52] P. Melki and R. Mulkern. "Magnetization transfer effects in multislice RARE sequences." In: *Magnetic Resonance in Medicine*. Vol. 24. 1. John Wiley & Sons, Inc, 1992, pp. 189–195.

[53] J. P. Tavares. "Otimização de Protocolos de Aquisição de Imagens de Ressonância Magnética Sensíveis à Concentração de Neuromelanina." Master's thesis. Faculty of Sciences and Technology, NOVA University of Lisbon, 2015.

[54] S. T. Schwarz, T. Rittman, V. Gontu, P. S. Morgan, N. Bajaj, and D. P. Auer. "T1-Weighted MRI shows stage-dependent substantia nigra signal loss in Parkinson's disease." In: *Movement Disorders*. Vol. 26. 9. John Wiley & Sons, Inc, 2011, pp. 1633–1638.

[55] K. Ogisu, K. Kudo, M. Sasaki, K. Sakushima, I. Yabe, H. Sasaki, S. Terae, M. Nakanishi, and H. Shirato. "3D neuromelanin-sensitive magnetic resonance imaging with semi-automated volume measurement of the substantia nigra pars compacta for diagnosis of Parkinson's disease." In: *Neuroradiology* 55.6 (2013), pp. 719–724.

[56] I. Natário. *Probabilidades e Estatística*. 2012.

[57] D. J. Sheskin. *Handbook of parametric and nonparametric statistical procedures*. 3rd ed. Boca Raton, Florida: CRC Press, 2003.

[58] V. Bewick, L. Cheek, and J. Ball. "Statistics review 10: further nonparametric methods." In: *Critical Care*. Vol. 8. 3. BioMed Central Ltd, 2004, pp. 196–199.

[59] E. Whitley and J. Ball. "Statistics review 6: Nonparametric methods." In: *Critical Care*. Vol. 6. 6. BioMed Central Ltd, 2002, pp. 509–513.

[60] T. K. Koo and M. Y. Li. "A guideline of selecting and reporting intraclass correlation coefficients for reliability research." In: *Journal of Chiropractic Medicine*. Vol. 15. 2. Elsevier, 2016, pp. 155–163.

[61] K. O. McGraw and S. P. Wong. "Forming inferences about some intraclass correlation coefficients." In: *Psychological Methods*. Vol. 1. 1. American Psychological Association, 1996, pp. 30–46.

[62] J. M. Bland and D. Altman. "Statistical methods for assessing agreement between two methods of clinical measurement." In: *The Lancet*. Vol. 327. 8476. Elsevier, 1986, pp. 307–310.

[63] D. Giavarina. "Understanding Bland Altman analysis." In: *Biochemia Medica* 25.2 (2015), pp. 141–151.

[64] N. G. Baikoussis, E. Apostolakis, N. A. Papakonstantinou, I. Sarantitis, and D. Dougenis. "Safety of magnetic resonance imaging in patients with implanted cardiac prostheses and metallic cardiovascular electronic devices." In: *The Annals of Thoracic Surgery*. Vol. 91. 6. Elsevier, 2011, pp. 2006–2011.

[65] A. M. Ferreira, F. Costa, A. Tralhão, H. Marques, N. Cardim, and P. Adragão. "MRI-conditional pacemakers: current perspectives." In: *Medical Devices: Evidence and Research*. Vol. 7. Dove Medical Press Ltd, 2014, pp. 115–124.

[66] A. J. Hughes, S. E. Daniel, L. Kilford, and A. J. Lees. "Accuracy of clinical diagnosis of idiopathic Parkinson's disease: a clinico-pathological study of 100 cases." In: *Journal of Neurology, Neurosurgery & Psychiatry* 55.3 (1992), pp. 181–184.

[67] D. J. Larkman and R. G. Nunes. "Parallel magnetic resonance imaging." In: *Physics in Medicine & Biology*. Vol. 52. 7. IOP Publishing Ltd, 2007, R15–R55.

[68] A. Rosset, L. Spadola, and O. Ratib. "OsiriX: an open-source software for navigating in multidimensional DICOM images." In: *Journal of Digital Imaging*. Vol. 17. 3. Springer, 2004, pp. 205–216.

[69] M. Fabbri, S. Reimão, M. Carvalho, R. G. Nunes, D. Abreu, L. C. Guedes, R. Bouça, P. P. Lobo, C. Godinho, M. Coelho, et al. "Substantia Nigra Neuromelanin as an Imaging Biomarker of Disease Progression in Parkinson's Disease." In: *Journal of Parkinson's Disease* 7.3 (2017), pp. 491–501.

[70] J. Langley, D. E. Huddleston, C. J. Liu, and X. Hu. "Reproducibility of locus coeruleus and substantia nigra imaging with neuromelanin sensitive MRI." In: *Magnetic Resonance Materials in Physics, Biology and Medicine*. Vol. 30. 2. Springer, 2017, pp. 121–125.

[71] M. Carvalho. "Estudo Imagiológico em Ressonância Magnética de doentes com Doença de Parkinson Late Stage." Master's thesis. Faculty of Sciences and Technology, NOVA University of Lisbon, 2016.

[72] M. Deeley, A Chen, R Datteri, J. Noble, A. Cmelak, E. Donnelly, A. Malcolm, L. Moretti, J Jaboin, K Niermann, et al. "Comparison of manual and automatic segmentation methods for brain structures in the presence of space-occupying lesions: a multi-expert study." In: *Physics in Medicine & Biology* 56.14 (2011), pp. 4557–77.

[73] J. R. Landis and G. G. Koch. "The measurement of observer agreement for categorical data." In: *Biometrics*. Vol. 33. 1. International Biometric Society, 1977, pp. 159–174.

[74] J. L. Fleiss, B. Levin, and M. C. Paik. *Statistical methods for rates and proportions*. 3rd ed. New York: John Wiley & Sons, Inc, 2013.

[75] S. B. Reeder, B. J. Wintersperger, O. Dietrich, T. Lanz, A. Greiser, M. F. Reiser, G. M. Glazer, and S. O. Schoenberg. "Practical approaches to the evaluation of signal-to-noise ratio performance with parallel imaging: Application with cardiac imaging and a 32-channel cardiac coil." In: *Magnetic Resonance in Medicine*. Vol. 54. 3. John Wiley & Sons, Inc, 2005, pp. 748–754.

[76] M. M. Goldenberg. "Medical management of Parkinson's disease." In: *Pharmacy and Therapeutics* 33.10 (2008), pp. 590–606.

[77] J. Meiser, D. Weindl, and K. Hiller. "Complexity of dopamine metabolism." In: *Cell Communication and Signaling*. Vol. 11. 34. BioMed Central Ltd, 2013, pp. 1–18.

[78] J. Dorszewska, M. Prendecki, M. Lianeri, and W. Kozubski. "Molecular effects of L-dopa therapy in Parkinson's disease." In: *Current Genomics*. Vol. 15. 1. Bentham Science Publishers, 2014, pp. 11–17.

[79] K. Westlund, R. Denney, R. Rose, and C. Abell. "Localization of distinct monoamine oxidase A and monoamine oxidase B cell populations in human brainstem." In: *Neuroscience*. Vol. 25. 2. Elsevier, 1988, pp. 439–456.

[80] P. D. Azevedo. "Quantificação de neuromelanina em doenças neurodegenerativas." Master's thesis. Faculty of Sciences and Technology, NOVA University of Lisbon, 2014.

[81] T. Hatano, A. Okuzumi, K. Kamagata, K. Daida, D. Taniguchi, M. Hori, H. Yoshino, S. Aoki, and N. Hattori. "Neuromelanin MRI is useful for monitoring motor complications in Parkinson's and PARK2 disease." In: *Journal of Neural Transmission*. Vol. 124. 4. Springer, 2017, pp. 407–415.

[82] M. J. Aminoff. "Pharmacologic Management of Parkinsonism & Other Movement Disorders." In: *Basic & Clinical Pharmacology*. 13th ed. New York, NY: McGraw-Hill Medical, 2015, pp. 447–61.

APPENDIX

Developed Interface

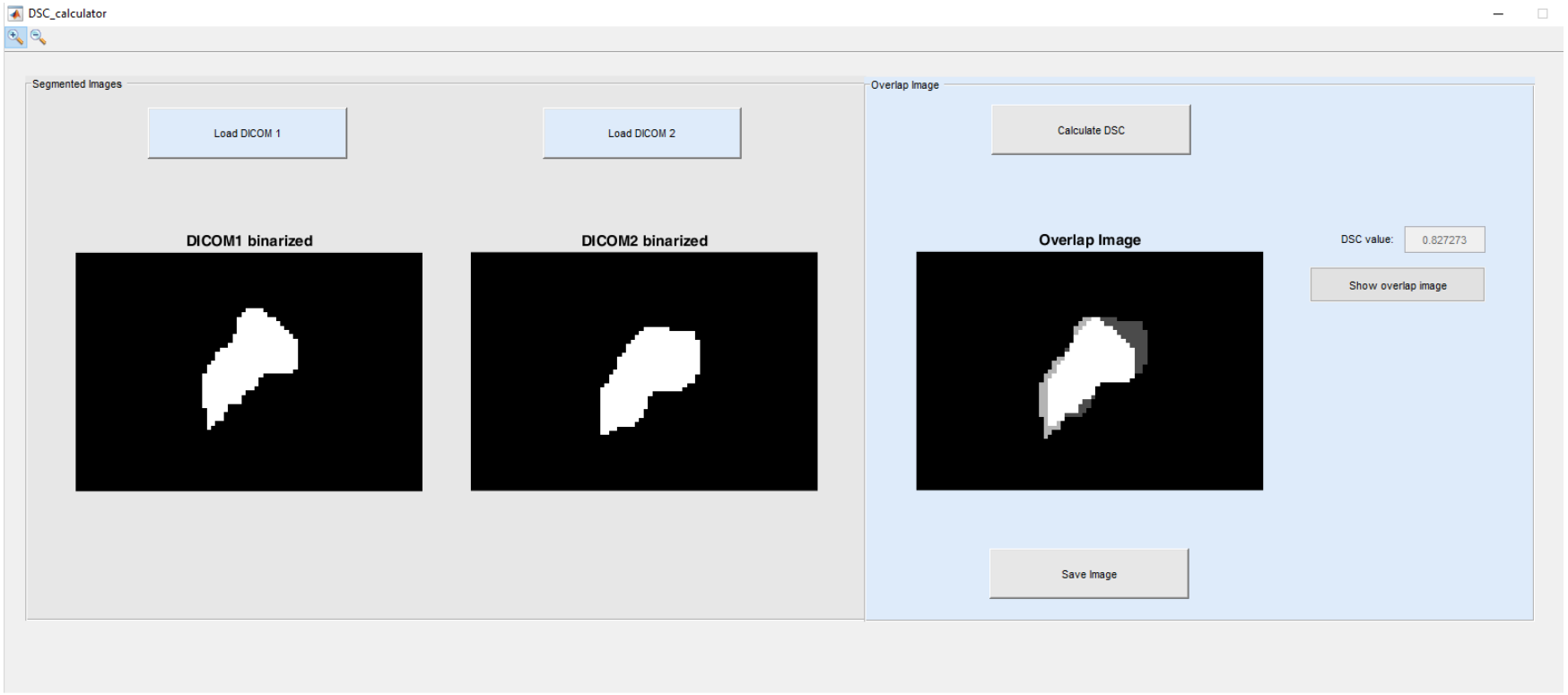

Figure A.1: Developed interface in Matlab for the Dice Similarity Coefficient calculation between two DICOMs containing segmented areas. The application enables the loading and visualization of two DICOM images and the visualization of the two segmented regions overlap. The application also enables the user to zoom in and out on all images and to save the resulted image.